Draft version December 8, 2020
Typeset using LaTeX **twocolumn** style in AASTeX63

Fast Optical Transients from Stellar-Mass Black Hole Tidal Disruption Events in Young Star Clusters

Kyle Kremer,[1,2,*] Wenbin Lu,[1] Anthony L. Piro,[2] Sourav Chatterjee,[3] Frederic A. Rasio,[4] and Claire S. Ye[4]

[1] *TAPIR, California Institute of Technology, Pasadena, CA 91125, USA*
[2] *The Observatories of the Carnegie Institution for Science, Pasadena, CA 91101, USA*
[3] *Tata Institute of Fundamental Research, Homi Bhabha Road, Navy Nagar, Colaba, Mumbai 400005, India*
[4] *Center for Interdisciplinary Exploration & Research in Astrophysics (CIERA) and Department of Physics & Astronomy, Northwestern University, Evanston, IL 60208, USA*

ABSTRACT

Observational evidence suggests that the majority of stars may have been born in stellar clusters or associations. Within these dense environments, dynamical interactions lead to high rates of close stellar encounters. A variety of recent observational and theoretical indications suggest stellar-mass black holes may be present and play an active dynamical role in stellar clusters of all masses. In this study, we explore the tidal disruption of main sequence stars by stellar-mass black holes in young star clusters. We compute a suite of over 3000 independent N-body simulations that cover a range in cluster mass, metallicity, and half-mass radii. We find stellar-mass black hole tidal disruption events (TDEs) occur at an overall rate of up to roughly $300\,\mathrm{Gpc}^{-3}\,\mathrm{yr}^{-1}$ in young stellar clusters in the local universe, with the majority occurring through binary–mediated dynamical encounters. These TDEs are expected to have several characteristic features, namely fast rise times of order a day, peak X-ray luminosities of at least $10^{44}\,\mathrm{erg\,s}^{-1}$, and bright optical luminosities (roughly $10^{41} - 10^{44}\,\mathrm{erg\,s}^{-1}$) associated with reprocessing by a disk wind. In particular, we show these events share many features in common with the emerging class of Fast Blue Optical Transients.

1. INTRODUCTION

The majority of stars are expected to form in young star clusters (YSCs; e.g., Carpenter 2000; Lada & Lada 2003). Several examples of YSCs exist in the Milky Way and the Local Group, and they are expected to be particularly abundant in starburst and interacting galaxies (e.g., Portegies Zwart et al. 2010). As dense stellar systems, YSCs undergo intense dynamical evolution governed by two-body relaxation, similar to their globular cluster (GC) cousins. Unlike GCs which are massive ($\sim 10^5 - 10^6\,M_\odot$) and old (ages of 10 Gyr or more), YSCs are generally low mass ($\lesssim 10^5\,M_\odot$) and short lived – many dissolve in the disk of their host galaxy on time scales of $\mathcal{O}(100\,\mathrm{Myr})$ (e.g., Kruijssen et al. 2011). However, before they dissolve, the stellar dynamical processes operating in YSCs make them efficient nurseries for many unusual astrophysical objects.

Over the past decade, the topic of stellar-mass black hole (BH) populations in stellar clusters has seen a boom in interest. On the observational side, a growing number of stellar-mass BH candidates have been observed in Milky Way GCs through both radial velocity measurements (Giesers et al. 2018, 2019) and through X-ray/radio observations (Maccarone et al. 2007; Strader et al. 2012; Chomiuk et al. 2013; Miller-Jones et al. 2015; Shishkovsky et al. 2018). On the theoretical side, state-of-the-art N-body modelling has shown that stellar-mass BHs form and are retained in stellar clusters of all masses (e.g., Morscher et al. 2015; Wang et al. 2015; Rodriguez et al. 2016; Banerjee 2017; Askar et al. 2018; Arca Sedda et al. 2018; Kremer et al. 2020a; Weatherford et al. 2019). Furthermore, cluster simulations have revealed that these BHs play a crucial role in the long-term dynamics, core evolution, and survival of stellar clusters (e.g., Mackey et al. 2007; Breen & Heggie 2013; Chatterjee et al. 2017; Kremer et al. 2018b; Ye et al. 2019; Kremer et al. 2019a; Giersz et al. 2019; Kremer et al. 2020a; Wang 2020).

One of the most exciting developments in the field of BH dynamics in stellar clusters lies in gravitational wave (GW) astrophysics. After formation, BHs are expected to rapidly sink to the center of their host cluster through dynamical friction (e.g., Kulkarni et al. 1993; Sigurdsson 1993; Morscher et al. 2015). Within their host cluster's dense core, BH–BH binaries form and subsequently harden through three-body dynamical encounters. Ultimately (depending on the host cluster's escape velocity), these binary BHs (BBHs) are either dynamically

Corresponding author: Kyle Kremer
kkremer@caltech.edu

* NSF Astronomy & Astrophysics Postdoctoral Fellow

ejected from their host cluster through gravitational recoil or merge inside their host cluster through GW inspiral. Recent studies have shown that YSCs (e.g., Ziosi et al. 2014; Di Carlo et al. 2019a; Banerjee 2020) and old GCs (e.g., Rodriguez et al. 2016; Rodriguez & Loeb 2018; Kremer et al. 2020a; Antonini & Gieles 2019) may contribute comparably to the overall BBH merger rate.

In addition to the applications to BBH formation and GW astronomy, stellar-mass BHs are also expected to dynamically interact with luminous stars in stellar clusters. BH–star encounters are expected to play a crucial role in the formation of both accreting and detached BH binaries (e.g., Ivanova et al. 2010, 2017; Kremer et al. 2018a; Giesler et al. 2018) with properties similar to the BH-candidates detected to date in Milky Way GCs (e.g., Kremer et al. 2019a). Additionally, such dynamical encounters may occasionally cause a star to cross a BH within its tidal disruption radius, leading to a tidal disruption of the star (Perets et al. 2016; Kremer et al. 2019d; Lopez et al. 2018; Samsing et al. 2019; Kremer et al. 2019b; Fragione et al. 2020). These stellar-mass BH tidal disruption events (TDEs) may occur during close encounters of pairs of single stars (i.e., single–single interactions) and also during small N (typically three- or four-body) resonant encounters that occur through binary-mediated dynamical interactions (e.g., Fregeau & Rasio 2007).

Regardless of the dynamical pathway, these TDEs are expected to lead to transients with fast rise times of roughly a day driven by viscous accretion onto the BH (e.g., Perets et al. 2016). Depending on the assumed accretion efficiency of the subsequently formed accretion disk, outflows associated with disk wind mass loss are expected to re-process the inner-disk radiation on a timescale of a few to 10 days, leading to peak bolometric luminosities up to roughly $10^{44}\,\mathrm{erg\,s^{-1}}$ that peak in the optical (Kremer et al. 2019d). In the case of extremely efficient energy release in the form of a jet, a bright X-ray or γ-ray flare may result with the overall phenomenology possibly resembling ultra-long gamma ray bursts (Perets et al. 2016). These TDEs are expected to occur in GCs at rates of roughly $3-10\,\mathrm{Gpc^{-3}\,yr^{-1}}$ (Perets et al. 2016; Lopez et al. 2018; Kremer et al. 2019d) and at similar rates in both nuclear star clusters (Fragione et al. 2020) and in stellar triples under the influence of Lidov-Kozai oscillations (Fragione et al. 2019).

In this paper, we examine the tidal disruption of main sequence stars by stellar-mass BHs in YSCs, in particular investigating the low-mass cluster regime, which is expected to dominate (by total number of clusters) the overall cluster mass function. This expands upon earlier work on the topic which was limited to old and massive GCs. We compile an extensive suite of N-body cluster models for various cluster masses and explore both TDE rates as well as characteristic properties.

Recent, current, and upcoming high-cadence surveys such as the Palomar Transient Factory (e.g., Law et al. 2009), the Zwicky Transient Facility (e.g., Bellm et al. 2019), ASAS-SN (e.g., Kochanek et al. 2017), ATLAS (e.g., Tonry et al. 2018), Pan-STARRs (e.g., Chambers et al. 2016), and the Vera Rubin Observatory (e.g., LSST Science Collaboration et al. 2009) are ushering in an unprecedented era in transient astronomy. Thus, the catalog of observed transients of both known and unknown origin is growing and will continue to grow rapidly. We conclude this study by examining the electromagentic features of stellar-mass BH TDEs and compare these events specifically with the emerging class of Fast Blue Optical Transients (FBOTs; e.g., Drout et al. 2014; Arcavi et al. 2016; Rest et al. 2018; Pursiainen et al. 2018; Margutti et al. 2019; Ho et al. 2020; Coppejans et al. 2020). On the basis of event rates, host galaxy properties, and overall transient features such as rise times and peak luminosities, we demonstrate stellar-mass BH TDEs may indeed be a viable mechanism for FBOTs.

In Section 2, we describe the methods we use to model stellar clusters. In Sections 3.1 and 3.2, we estimate TDE rates occurring through single–single and binary-mediated encounters, respectively, and compare the rates estimated from our N-body models with simple analytic estimates. In Section 3.3, we compute the overall TDE rates at various cosmological distances and in Section 3.4, we describe how TDE properties may vary with cluster metallicity. In Section 4, we discuss of the expected outcome of stellar-mass BH TDEs, specifically describing the basic properties of disk formation and evolution and the associated electromagnetic signatures. We also compare these features with observed properties of FBOTs. We discuss our results and conclude in Section 5.

2. N-BODY MODELS OF YOUNG CLUSTERS

To model the evolution of young star clusters, we use the Hénon-type Monte Carlo code `CMC` (Joshi et al. 2000; Pattabiraman et al. 2013; Kremer et al. 2020a). `CMC` includes various physical processes necessary to study both large scale cluster dynamics and the formation and evolution of stellar-mass BHs, including two-body relaxation, stellar and binary star evolution (computed using updated versions of `SSE` and `BSE`; Hurley et al. 2000, 2002), and direct integration of small-N resonate encounters (Fregeau & Rasio 2007) including post-Newtonian effects (Rodriguez et al. 2018).

To compute compact object (BH and neutron star) masses, we adopt the stellar wind prescriptions of Vink et al. (2001) to determine the final stellar mass at the moment of core collapse and adopt the "Rapid" SNe explosion models (Fryer et al. 2012) to compute neutron star and BH masses modified to include the prescriptions for (pulsational) pair-instability supernovae described in Belczynski et al. (2016). BH and NS natal kicks are computed as in Kremer et al. (2020a).

Table 1. List of N-body models

[1]Label	[2]N ($\times 10^4$)	[3]$M_{\rm cl}$ ($\times 10^4\,M_\odot$)	[4]num. of models	[5]r_v (pc)	[6]Z ($Z_\odot$)	[7]$t_{\rm max}$ (Myr)	[8]single–single TDEs	[9]binary–single TDEs
a	1	0.6	1000	1	1	150	6	11
b	2	1.2	400	1	1	150	8	7
c	4	2.4	300	1	1	150	11	9
d	6	3.6	300	1	1	500	75	91
e	8	4.8	200	1	1	500	83	59
f	10	6.0	150	1	1	500	100	53
g	20	12	100	1	1	500	187	61
h	80	48	10	1	1	500	182	15
i	8	4.8	200	1	0.1	500	122	78
j	10	6.0	150	1	0.1	500	170	58
k	20	12	100	1	0.1	500	238	61
l	10	12	50	0.42	1	500	128	138
m	10	12	50	0.42	0.1	500	156	61

Note—All models computed in this study. In columns 2 and 3 we list the initial number of stars and cluster mass, respectively. In column 4, we list the total number of independent realizations computed for the given set of initial conditions. In columns 5, 6, and 7, we list the initial virial radius, metallicity, and maximum integration time, respectively. In columns 8 and 9, we list the total number of TDEs occuring through single–single and binary–single encounters respectively.

As discussed in Section 1, a natural outcome of dynamical interactions between stellar-mass BHs and stars is tidal disruption of the star. In order to treat stellar-mass BH TDEs, we adopt the same prescriptions as in Kremer et al. (2019d). In short, if a dynamical encounter involving at least one BH and one star[1] leads to a BH–star pericenter passage, r_p, within the star's tidal disruption radius

$$r_{\rm TD} = \left(\frac{m_{\rm BH}}{m_\star}\right)^{1/3} R_\star, \tag{1}$$

where $m_{\rm BH}$ is the BH mass, and $m_\star$ and $R_\star$ are the stellar mass and radius, respectively, we assume a TDE occurs.[2] At this point, we record the stellar properties and then assume the star is instantaneously destroyed. In reality, especially if the TDE occurs during a multi-body resonant encounter, TDEs may affect the hydrodynamic evolution of their dynamical encounters. These more complex effects are well beyond the computational scope of an N-body code like `CMC`, but see e.g., Lopez et al. (2018) for discussion.

[1] Here, we are specifically interested in disruption of *main sequence* stars. Henceforth, we use the term "star" to mean a main sequence star. For discussion of the interaction of BHs with giants, see Ivanova et al. (2010, 2017); Kremer et al. (2019d).

[2] In reality, the tidal disruption radius of a particular object likely depends also upon the object's stellar structure. In particular, this dependence may change as stars evolve and develop a more pronounced core-envelope structure. We reserve inclusion of these more detailed effects for future study and note that these effects are unlikely to affect the results presented here significantly.

We apply this TDE prescription only for BH–star interactions. For close encounters of star–star pairs, we allow the stars to interact only in the direct collision limit: we assume a sticky sphere collision (i.e., zero mass loss) occurs if $r_p < R_1 + R_2$, where R_1 and R_2 are the stellar radii. See Kremer et al. (2020b) for further details of our treatment of star–star collisions. We record TDEs/collisions that occur during both single–single encounters and binary-mediated dynamical encounters that are integrated directly using `Fewbody`. For further detail, see Fregeau & Rasio (2007); Kremer et al. (2019d, 2020b).

In all models, we assume a static Milky-Way-like external tidal field representative of the solar neighborhood (i.e., located at a distance of 8 kpc from the Galactic center). In reality, this choice likely underestimates the role of external tides on the long-term cluster evolution as it does not incorporate the effects of massive perturbers (e.g. molecular clouds), which may accelerate the cluster disruption (e.g., Gieles et al. 2006). We do not model here the dynamics of the final phase of cluster dissolution. As in Di Carlo et al. (2019a), we integrate our clusters to a maximum age of $150-500$ Myr, depending on the cluster mass (allowing more massive clusters to evolve longer to reflect their long relaxation times; e.g., Heggie & Hut 2003). Indeed, assuming a maximum age of 500 Myr is appropriate as our focus here lies primarily on young clusters as opposed to long-lived globular clusters with ages of 10 Gyr or more (see Portegies Zwart et al. 2010, for further discussion). Furthermore, real star clusters are formed in a complicated interaction between gas and gravity (e.g., Bate et al.

2003), which, in general, is poorly understood. In CMC, we neglect the initial gas-rich phase of cluster evolution and instead assume a single starburst creates all stars. In particular, we do not consider expulsion of primordial gas that occurs on a dynamical timescale at early times and the possible consequences on the cluster dynamics/survival (e.g., the "infant mortality" effect; Lada & Lada 2003).

We consider initial cluster masses in the range $6000 - 6 \times 10^5\,M_\odot$, reflective of the YSC masses observed in local universe (e.g., Lada & Lada 2003; Portegies Zwart et al. 2010). For all models, we adopt a standard Kroupa (2001) initial mass function with a mass range of $0.08 - 150\,M_\odot$. We assume all models are initially fit to a King model with concentration parameter $W_0 = 5$ (King 1962).

We adopt two values for the cluster initial virial radius, r_v. In the first limit, we assume a constant $r_v = 1\,\mathrm{pc}$ for all cluster masses (e.g., Portegies Zwart et al. 2010). In the second limit, we follow the phenomenological results of Marks et al. (2012) which showed cluster half-mass radii, r_h (a reasonable proxy for r_v), exhibit a weak dependence on total cluster mass:

$$r_\mathrm{h} = 0.1^{+0.07}_{-0.04}\,\mathrm{pc}\left(\frac{M_\mathrm{cl}}{M_\odot}\right)^{0.13\pm0.04}. \quad (2)$$

As the virial radii given by the Equation 2 are a factor of roughly two smaller than the $r_v = 1\,\mathrm{pc}$ assumption, the models adopting this relation are roughly an order of magnitude denser than the $r_v = 1\,\mathrm{pc}$ counterparts. In this case, the various dynamical processes, including stellar-mass BH TDEs occur at an increased rate under the Marks et al. (2012) assumption, as will be discussed further in Section 3.

For simplicity, we assume zero primordial stellar binaries in all models in this study. Under this assumptions, all TDEs occur as a result of well-understood dynamical processes, with no assumptions required regarding the uncertain properties of primordial stellar binaries in clusters. However, if indeed primordial binaries are present, this will likely lead to an increase TDE rate (for example, see Fregeau & Rasio 2007, which explored the role of primordial binaries in the similar topic of stellar collisions). In this case, the results of this study may be viewed as a conservative lower limit on the true TDE rate in YSCs.

Finally, to increase the robustness of our results, we run a large number of independent realizations of each set of cluster initial conditions. In total, we produce 3010 independent models. The complete list of models, including initial conditions and numbers of TDEs, is shown in Table 1.

3. RESULTS

In this section, we show the results of our suite of N-body models. In Sections 3.1 and 3.2, we discuss TDEs that occur during single–single and binary–single dynamical encounters, respectively, and compare to simple analytic estimates. In Section 3.3, we examine the properties of TDEs and how these properties vary with both the cluster metallicity and initial density. Finally, in Section 3.4, we estimate the overall rates of TDEs at various redshifts.

3.1. *Single–single TDEs*

We first discuss the case of TDEs occuring during single–single encounters between a BH and a MS star. For a given cluster with N total stars and half-mass radius r_h, the rate of TDEs occurring through single–single dynamical encounters can be estimated as

$$\Gamma_\mathrm{ss} \approx n_\star \Sigma_\mathrm{ss} \sigma_v N_\mathrm{BH} \quad (3)$$

where N_BH is the total number of BHs in the cluster (which, in general, are all found within the half-mass radius due to mass segregation; e.g., Morscher et al. 2015), $n_\star \approx N/r_\mathrm{h}^3$ is the number density, and σ_v is the cluster's velocity dispersion. Σ_ss is the cross section for a single–single TDE, given by

$$\Sigma_\mathrm{ss} = \pi R_\mathrm{TD}^2 \left[1 + \frac{2G(m_\mathrm{BH} + m_\star)}{R_\mathrm{TD}\sigma_v^2}\right] \quad (4)$$

where m_BH and $m_\star$ are the typical BH and stellar masses and R_TD is the tidal disruption radius given by Equation 1. For a cluster with a Kroupa (2001) IMF, we can take $m_\star \approx 0.6\,M_\odot$. For high-metallicity clusters ($Z \approx Z_\odot$), we can take $m_\mathrm{BH} \approx 10\,M_\odot$, while for low-metallicity clusters ($Z \lesssim 0.1 Z_\odot$), $m_\mathrm{BH} \approx 25\,M_\odot$ is more appropriate (e.g., Kremer et al. 2020a).

Assuming the cluster is initially in virial equilibirum ($\sigma_v \approx \sqrt{GM_\mathrm{cl}/r_\mathrm{h}}$, where $M_\mathrm{cl} \approx m_\star N$ is the total cluster mass), assuming all encounters occur in the gravitational focusing regime (the second term in the brackets of Equation 4 dominates), and taking $m_\mathrm{BH} \gg m_\star$, we can rewrite Equation 3 as

$$\Gamma_\mathrm{ss} \approx 0.2\,\mathrm{Gyr}^{-1}\left(\frac{M_\mathrm{cl}}{10^4\,\mathrm{M}_\odot}\right)^{1/2}\left(\frac{r_\mathrm{h}}{1\,\mathrm{pc}}\right)^{-5/2} \times \left(\frac{m_\star}{0.6\,M_\odot}\right)^{-4/3}\left(\frac{m_\mathrm{BH}}{10\,M_\odot}\right)^{4/3}\left(\frac{R_\star}{0.6\,R_\odot}\right)\left(\frac{N_\mathrm{BH}}{10}\right). \quad (5)$$

For a Kroupa (2001) IMF, we expect roughly 10^{-3} BHs to form per star, giving us $N_\mathrm{BH} \approx 10^{-3} N$. In this case, we obtain the analytic scaling

$$\Gamma_\mathrm{ss} \approx 0.2\,\mathrm{Gyr}^{-1}\left(\frac{M_\mathrm{cl}}{10^4\,M_\odot}\right)^{3/2}. \quad (6)$$

In Figure 1 we show as open circles the rates of such encounters as a function of cluster mass as determined from our N-body models. To isolate specifically the effect of cluster mass, we utilize only the first 8 sets of simulations listed in Table 1 (models a-h), which have

fixed metallicity ($Z_\odot$) and virial radius (1 pc). To calculate the model rates, we simply count the total number of single–single TDEs in all models of a given cluster mass, then divide by the total number of models and by the total integration time for the given cluster mass (see Table 1). Error bars denote 2σ from the mean, assuming a Poisson distribution.

From a least squares fit, we find these data are best fit by the power-law relation

$$\Gamma_{\rm ss}^{\rm model} = 0.07 \pm 0.01\,{\rm Gyr}^{-1}\left(\frac{M_{\rm cl}}{10^4\,{\rm M}_\odot}\right)^{1.6\pm0.16}. \quad (7)$$

This fit is shown as the blue curve in Figure 1, with the blue bands denoting the 90% confidence interval from the least squares fit. For comparison, we show as the dashed gray line in Figure 1 the $\Gamma \propto M_{\rm cl}^{3/2}$ scaling relation derived from the simple analytic estimate in Equation 6.

In Equation 6, we have assumed a constant $r_{\rm h} \approx 1$ pc is typical for all YSCs (see, e.g., Portegies Zwart et al. 2010). Alternatively, as discussed in Section 2, $r_{\rm h} < 1$ pc may be more appropriate and furthermore, $r_{\rm h}$ may exhibit a weak dependence on total cluster mass. To explore the possibility, we ran an additional set of models (group `l` in Table 1) with initial $r_v = 0.42$ pc, reflective of the $r_{\rm h} - M_{\rm cl}$ relation of Marks et al. (2012). Given the phenomenological relation from Marks et al. (2012) predicts cluster radii a factor of roughly 2 lower than the $r_{\rm h} = 1$ pc assumption, the following rate, $\Gamma_{\rm ss}^{\rm phenom}$, is higher than that estimated from Equation 7.

Combining the phenomenological $r_{\rm h} - M_{\rm cl}$ relation of Marks et al. (2012) (Equation 2) with Equations 3 and 4, we expect $\Gamma_{\rm ss}^{\rm phenom} \propto M_{\rm cl}^{1.175}$. Scaling to the rate identified from the models in group `l`, we can then write:

$$\Gamma_{\rm ss}^{\rm phenom} \approx 0.63\,{\rm Gyr}^{-1}\left(\frac{M_{\rm cl}}{10^4\,M_\odot}\right)^{1.175}. \quad (8)$$

3.2. *Binary-mediated TDEs*

In addition to TDEs occurring through single–single encounters, TDEs may also take place during binary-mediated resonant encounters involving at least one BH and one star. As discussed in Section 2, we do not include stellar binaries in this study. The only binaries formed are BH binaries assembled through three-body encounters (for simplicity, three-body binary formation is allowed *only* for BHs in our models; e.g., Morscher et al. 2015). In this case, the binary-mediated TDEs discussed in this subsection are those that occur specifically during binary–single resonant encounters between a BBH and a single MS star.

Using a similar calculation to that performed for the single–single rate estimate, the rate of TDEs during BBH–star binary–single encounters can be written as

$$\Gamma_{\rm bs} \approx n_\star\,\Sigma_{\rm bs}\,\sigma_v\,N_{\rm BBH}\,P_{\rm TD}. \quad (9)$$

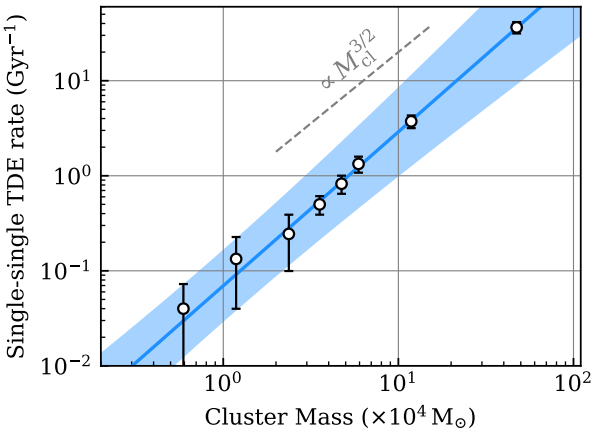

Figure 1. TDE rate per cluster as a function of initial cluster mass using models `a-h` in Table 1 (assuming $r_h = 1$ pc). Open circles denote rates computed from the suite of N-body models and the solid blue curve shows the best-fit relation of Equation 7. The shaded blue region denotes the 90% confidence interval from the least squares fit. The dashed gray line shows the $\propto M_{\rm cl}^{3/2}$ analytic scaling from Equation 6.

Here $\Sigma_{\rm bs}$ is the cross section for binary–single encounters

$$\Sigma_{\rm bs} = \pi a_{\rm BBH}^2\left[1 + \frac{2G(m_{\rm BBH} + m_\star)}{a_{\rm BBH}\sigma_v^2}\right] \quad (10)$$

where $a_{\rm BBH}$ is the BBH semi-major axis and $m_{\rm BBH} \approx 2m_{\rm BH}$ is the mass of the BBH. $N_{\rm BBH}$ is the total number of BBHs in the cluster. As shown in a number of recent analyses (e.g., Morscher et al. 2015; Chatterjee et al. 2017; Banerjee 2018), $N_{\rm BBH}$ is expected to be roughly independent of the total number of BHs in the cluster as well as the cluster's total mass, such that the total number of dynamically-formed BBHs present at any given time never exceeds a few. Here assume $N_{\rm BBH} \approx 2$.

Finally, $P_{\rm TD}$ is the probability that a given BBH–star resonant encounter leads to a TDE. We follow the results of Darbha et al. (2018), which showed that for asymmetric mass ratio binary-single encounters, $P_{\rm TD}$ is roughly proportional to $R_{\rm TD}/a_{\rm BBH}$. Note that this same scaling is found in the equal mass case (e.g., Samsing et al. 2017; Samsing 2018). Here we take $P_{\rm TD} = 2R_{\rm TD}/a_{\rm BBH}$ as in Samsing et al. (2019). We can then rewrite Eq. 9 as

$$\Gamma_{\rm bs} \approx 0.3\,{\rm Gyr}^{-1}\left(\frac{M_{\rm cl}}{10^4\,{\rm M}_\odot}\right)^{1/2} \quad (11)$$

where, as before, we have assumed $r_{\rm h} \approx 1$ pc, $m_{\rm BH} \approx 10\,M_\odot$, $m_\star \approx 0.6\,M_\odot$, and $R_\star \approx 0.6\,R_\odot$, independent of the cluster mass.

Comparing to Equation 6, we find $\Gamma_{\rm bs}/\Gamma_{\rm ss} \propto N_{\rm BH}^{-1} \propto M_{\rm cl}^{-1}$. Thus, lower-mass clusters with fewer BHs feature

a higher BBH TDE rate per BH (and therefore also per star) compared to higher-mass clusters with more BHs. Thus, given that lower-mass clusters also dominate by number the overall cluster mass function, they are the ideal environment to find BBH TDEs. We return to the question of overall and relative rates in Section 3.3.

In Figure 2 we show the rates of these events as a function of cluster mass as determined from our N-body models. As in Figure 1, the rate is computed as the total number of binary–single TDEs in all models of a given cluster mass, divided by the total number of models and by the time duration, Δt. Unlike in the single–single case, where the necessary dynamical encounters begin immediately, in the binary–single case we must first wait for BHs to mass-segregate to the center so that the target BBHs can form through three-body encounters. For each model, we define this timescale, $t_{\rm 3bb}$, simply as the moment the first BBH forms in that model. Then, $\Delta t = t_{\rm max} - t_{\rm 3bb}$. Typically, $t_{\rm 3bb}$ is of order 100 Myr (see also Sigurdsson 1993; Morscher et al. 2015).

Again performing a least squares fit, we find these data are best fit by the power-law relation

$$\Gamma_{\rm bs}^{\rm model} = 0.69 \pm 0.36\,{\rm Gyr}^{-1}\left(\frac{M_{\rm cl}}{10^4\,{\rm M}_\odot}\right)^{0.3\pm0.09}, \quad (12)$$

which can be compared with the simple analytic estimate of Eq. 11. As with the single–single case, we find the analytic estimate recovers reasonably well the rate inferred from the N-body modelling.

As before, we can also estimate a phenomenological rate, $\Gamma_{\rm bs}^{\rm phenom}$, assuming the relation of Marks et al. (2012). Combining Equations 2 and 11, we expect $\Gamma_{\rm bs}^{\rm phenom} \propto M_{\rm cl}^{0.175}$. Again normalizing to the binary–single TDE rate estimated in the models form group `1` in Table 1, we can write

$$\Gamma_{\rm bs}^{\rm phenom} \approx 4.4\,{\rm Gyr}^{-1}\left(\frac{M_{\rm cl}}{10^4\,{\rm M}_\odot}\right)^{0.125}. \quad (13)$$

Because we assume that BH binaries form exclusively through three-body encounters, Equations 12 and 13 are relevant only for those clusters with at least three BHs at birth, so that at least one BBH can form. Again, assuming roughly 1 BH forms per 1000 stars (Kroupa 2001), this requires $N \gtrsim 3000$ or $M_{\rm cl} \gtrsim 2000\,M_\odot$. For clusters with $M_{\rm cl} \lesssim 2000\,M_\odot$, Equations 12 and 13 are no longer applicable and the binary–single TDE rate is zero. We return to this point in Section 3.3 when we compute the total TDE rate by integrating over the full cluster mass function.

3.2.1. *Binary BH orbital separations*

Given that the binary–single TDE rate is expected to be roughly independent of the binary orbital separation, the distribution of $a_{\rm BBH}$ for BBHs that undergo TDEs is expected to follow the semi-major axis for all BBHs in a cluster of a given mass (e.g., Samsing et al. 2019; Kremer et al. 2019c). In Figure 3, we show the distribution of $a_{\rm BBH}$ for all BBHs found in our models of various initial masses. These distribtions are determined by two primary physical processes:

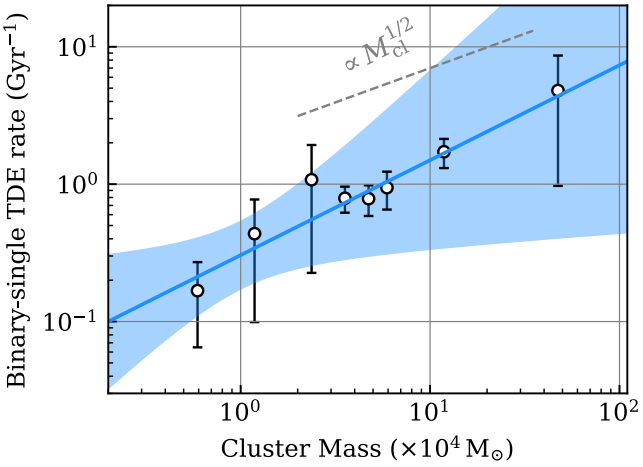

Figure 2. Same as Figure 1 but for TDEs occurring during binary–single encounters. Here the blue curve shows the best-fit relation of Equation 13 and the dashed gray line shows the $\propto M_{\rm cl}^{1/2}$ analytic scaling from Equation 11.

Three-body formation: The maximum semi-major axis of a binary formed through a three-body encounter is determined by the hard-soft boundary $a_{\rm HS} \propto m_{\rm BH}/\sigma_v^2$ (e.g., Morscher et al. 2015). Assuming $\sigma_v^2 \propto M_{\rm cl}$, we expect, in general, more massive clusters will produce more compact BBHs compared to lower mass clusters.

Ejection from dynamical recoil: Once a BBH is formed, it will (on average) harden through subsequent binary-mediated encounters with other BHs and stars in the cluster core (e.g., Sigurdsson 1993; Morscher et al. 2015; Rodriguez et al. 2016). Following a dynamical encounter, the BBH will receive a dynamical recoil kick with a magnitude comparable to the BBH orbital velocity, $v_{\rm recoil}^2 \propto a_{\rm BBH}^{-1}$. Thus, as a BBH hardens, it attains increasingly large dynamical recoil kicks. Eventually, $v_{\rm recoil}$ is sufficiently large for the binary to be ejected from the cluster. This is set by the cluster's escape velocity $v_{\rm esc}^2 \propto M_{\rm cl}/r_{\rm h}$. As a result, in lower-mass clusters, BBHs will be dynamically ejected before they can harden as far as is possible in higher-mass clusters.

As a consequence of these two processes, we expect the BBH semi-major axis distribution to shift toward lower values in increasingly massive clusters. Indeed, this is shown in Figure 3.

One exciting possibility proposed in Lopez et al. (2018); Samsing et al. (2019); Kremer et al. (2019c) is that these binary-mediated TDEs may be used to indirectly probe properties of the underlying BBH population, if the corresponding electromagnetic (EM) signal can be detected. The basic idea is the second BH pro-

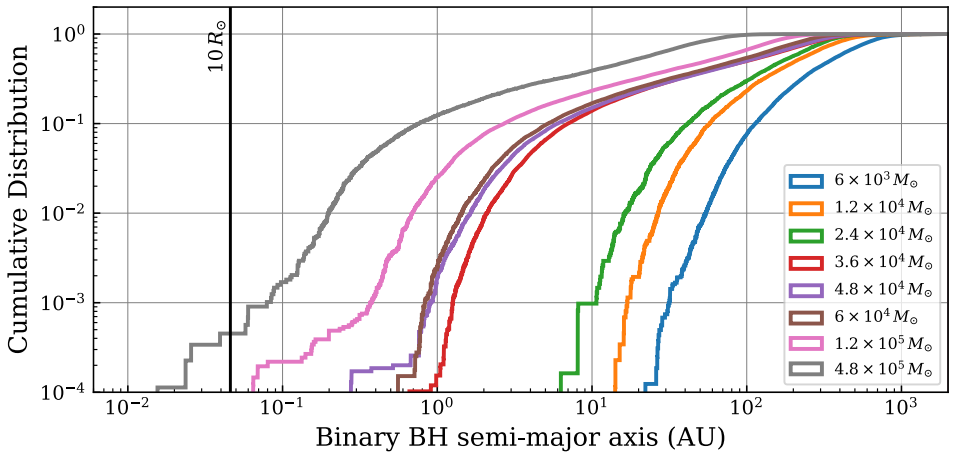

Figure 3. Cumulative distribution of semi-major axis for all BBHs identified in our models. The various colors denote different cluster masses. As shown, more massive clusters host, on average, more compact BBHs. The solid black line shows the characteristic orbital separation at which the BH binary companion may interrupt the TDE lightcurve, as described in the text.

duces breaks in the lightcurve on timescale comparable to the BBH orbital period. This idea has been illustrated in the supermassive BH (SMBH) regime using numerical techniques (e.g., Liu et al. 2009; Coughlin et al. 2017), and one SMBH candidate has proposed (TDE J1201+30), from which the authors were able to constrain the SMBH binary orbital period Liu et al. (2014). This process likely requires the $a_{\rm BBH}$ to be comparable to the disk radius, which in turn will be comparable to the tidal disruption radius. For reference, we show $r_{\rm TD} \approx 10\,R_\odot$ as a solid black line in Figure 3 (see Equation 1). As shown in the figure, this process is likely only possible in the most massive clusters explored here ($M_{\rm cl} \gtrsim 10^5\,M_\odot$). Even for our massive cluster simulations, we find that only $\approx 0.1\%$ of all BBHs meet this criterion. Thus, we conclude that the presence of a second BH is unlikely to significantly affect the TDE dynamics and subsequent lightcurve evolution.

Although it appears this possibility is not relevant in typical YSCs, we can speculate that more massive clusters such as nuclear star clusters with masses of $10^7\,M_\odot$ or larger may be ideal environments for this processes, given that more massive clusters should be able to host even more compact BBHs. We reserve a more detailed study of this possibility for future study, and direct the reader to Fragione et al. (2020) for a discussion of TDEs in the nuclear star cluster regime.

3.3. *Estimating the total event rate*

The functional form for the initial mass function of YSCs is expected to be well-represented by a power-law distribution (e.g., Lada & Lada 2003) with a possible exponential truncation above cluster masses of roughly $M_{\rm cut} \approx 10^6\,M_\odot$ (e.g., Portegies Zwart et al. 2010):

$$\frac{dN}{dM_{\rm cl}} \propto M_{\rm cl}^{-2} \exp(-M_{\rm cl}/M_{\rm cut}). \tag{14}$$

As we are interested here primarily in the low-mass tail of the mass function ($\lesssim 10^5\,M_\odot$), the specific value of $M_{\rm cut}$ is not relevant to this study.

We can then compute the total TDE rate from a realistic population of YSCs in Milky Way-like galaxies by integrating the rate per cluster (Eq. 5) over the cluster mass function:

$$\Gamma_{\rm tot} = \int_{M_{\rm low}}^{M_{\rm high}} \frac{\Gamma_{\rm cl}}{M_{\rm cl}} \frac{dN}{dM_{\rm cl}}\,\Delta t\,\rho_{\rm SF}\,f_{\rm SF}\,dM_{\rm cl}. \tag{15}$$

The integration limits represent the assumed range in cluster masses; we assume $M_{\rm low} = 100\,M_\odot$ and $M_{\rm high} = 10^5\,M_\odot$ (Lada & Lada 2003). By definition, in order for TDEs to occur through the binary–single channel discussed in Section 3.2, BBHs must have formed in the cluster. As discussed in Section 3.2, because we assume that BBHs form exclusively through three-body encounters, this requires at least three BHs be present in the cluster at birth, which in turn requires $M_{\rm cl} \gtrsim 2000\,M_\odot$. Thus, to compute the rate of TDEs occurring through binary–single encounters, we use $M_{\rm low} = 2000\,M_\odot$ (keeping the overall normalization of Equation 14 the same as before). Note that this mass requirement automatically takes care of the additional requirement that the cluster not dissolve before the first BBHs begin to form.

Δt is the assumed timespan over which TDEs may occur. For short-lived clusters, Δt is simply lifetime of the cluster before evaporation through its tidal boundary. In reality, this timescale depends upon the location of the cluster in its host galaxy's tidal field, as well as on more complex phenomena such as, e.g., tidal shocks and interactions with giant molecular clouds as mentioned in Section 2. In lieu of consideration of these more detailed effects, we simply adopt the relation in Binney &

Tremaine (1987), where the evaporation timescale can be expressed as

$$t_{\rm evap} \approx f t_{\rm rh}. \quad (16)$$

Here, $t_{\rm rh}$ is the cluster's half-mass relaxation time

$$t_{\rm rh} = \frac{0.17N}{\log\Lambda}\sqrt{\frac{r_{\rm h}^3}{GM_{\rm cl}}} \quad (17)$$

where $\log\Lambda$ is the Coulomb logarithm, which we approximate as $\log(0.1N)$. For clusters with tidal radii and other properties similar to Milky Way clusters, the coefficient f is expected to lie in the range 20-60 (e.g., Spitzer 1987; Gnedin et al. 1999). Here, we take $f = 20$. Again, as we are specifically interested in young clusters with ages less than roughly 500 Myr, we take

$$\Delta t = \min\left(t_{\rm evap}, 500\,{\rm Myr}\right) \quad (18)$$

For TDEs occurring during binary–single encounters, we must also incorporate the timescale for BBH formation to begin. In Section 3.2, we computed this timescale directly from the models. Here, for simplicity (and as motivated by the results from the models), we assume BBH formation occurs after roughly 100 Myr for all cluster masses (see also, e.g., Sigurdsson 1993). In this case, for binary–single TDEs, $\Delta t = \min(t_{\rm evap}, 500\,{\rm Myr}) - 100\,{\rm Myr}$.

$\rho_{\rm SF}$ is the assumed cosmological density of star formation rate (SFR). We adopt the SFR of Hopkins & Beacom (2006). Specifically, this study finds $\rho_{\rm SF}/[M_\odot\,{\rm yr}^{-1}\,{\rm Mpc}^{-3}] = 1.5\times10^{-2}$, 0.1, and 0.2 at redshift $z = 0, 1$, and 2.5 (peak star formation), respectively. $f_{\rm SF}$ is the fraction of the star formation rate assumed to occur in star clusters. For low-mass clusters ($M_{\rm cl} < 10^5\,\odot$) we assume $f_{\rm SF} = 0.8$ (Lada & Lada 2003).

Finally, Γ is the TDE rate per cluster of a given mass, $M_{\rm cl}$. For this we adopt the scaling relations derived in Section 3 (Equations 7 and 12, for the single–single and binary–single cases, respectively, assuming constant $r_{\rm h} = 1\,{\rm pc}$). Additionally, we use Equations 8 and 13 to compute the rates assuming higher density YSCs as in the phenomenological fits of Marks et al. (2012).

We present in Table 2 the rate estimates obtained by integrating Equation 15. We find that the binary–single channel dominates over the single–single channel by a factor of roughly a few to ten, depending upon the assumptions made regarding $r_{\rm h}$. If we adopt the more conservative choice of constant $r_{\rm h} = 1\,{\rm pc}$, we estimate a combined TDE rate of roughly $30\,{\rm Gpc}^{-3}\,{\rm yr}^{-1}$ in the local universe. Adopting the phenomenological assumption from Marks et al. (2012), we find a combined TDE rate of roughly $300\,{\rm Gpc}^{-3}\,{\rm yr}^{-1}$.

For reference, Kremer et al. (2019d) predicted a TDE rate of roughly $10\,{\rm Gpc}^{-3}\,{\rm yr}^{-1}$ for old globular clusters.

Table 2. Volumetric TDE rates

$r_{\rm h}$ prescription	$z=0$	$z=1$	$z=2.5$
	$({\rm Gpc}^{-3}\,{\rm yr}^{-1})$		
Single–single TDE rate:			
$r_{\rm h} = 1\,{\rm pc}$	2.0	13.6	23.2
Marks et al. 2012	79.0	526.7	895.4
Binary–single TDE rate:			
$r_{\rm h} = 1\,{\rm pc}$	25.6	171.1	290.9
Marks et al. 2012	214.4	1429.6	2430.3

NOTE—Volumetric event rates of TDEs occurring through both single-single and binary-single encounters in YSCs in the local universe ($z = 0$), at $z = 1$, and at peak star formation ($z \approx 2.5$). We show both rates calculated assuming constant cluster half-light radii, $r_{\rm h} = 1\,{\rm pc}$ and assuming the $r_{\rm h} - M_{\rm cl}$ relation of Marks et al. (2012) (Equation 2).

In the more massive nuclear star cluster regime, Fragione et al. (2020) predicted a stellar-mass BH TDE rate of roughly $10^{-7} - 10^{-6}\,{\rm yr}^{-1}$ per galaxy. Assuming a galactic density of roughly $10^{-2}\,{\rm Mpc}^{-3}$, this corresponds to a rate of roughly $1 - 10\,{\rm Gpc}^{-3}\,{\rm yr}^{-1}$ in the local universe. Thus, we conclude YSCs may dominate the overall stellar-mass BH TDE rate in the local universe by a factor of a few to more than an order of magnitude compared to more massive clusters.

3.4. *BH mass function of TDEs*

In the previous subsections, we have explored specifically models `a-h` of Table 1 which assume solar metallicity, reflective of YSCs born recently in the local universe. However, for YSCs found at higher redshifts, assuming a lower metallicity is more appropriate. Given the overall TDE rate be substantially higher at high redshift (see Section 3.3), a careful investigation of metallicity is warranted.

To explore the effect of cluster metallicity on TDE properties, we have run several additional sets of models with $Z = 0.1Z_\odot$. In Figure 4, we show the distribution of BH masses that undergo TDEs. The black and hatched gray histograms show BH masses found in models assuming $r_{\rm h} = 1\,{\rm pc}$ and the Marks et al. (2012) $r_{\rm h}-M_{\rm cl}$ relation, respectively. In the top (bottom) panel we show the results for models assuming solar (10% solar) metallicity.

The first general feature we see is that higher metallicity clusters yield lower mass BH TDEs. This is anticipated: at higher metallicity, stellar winds are expected

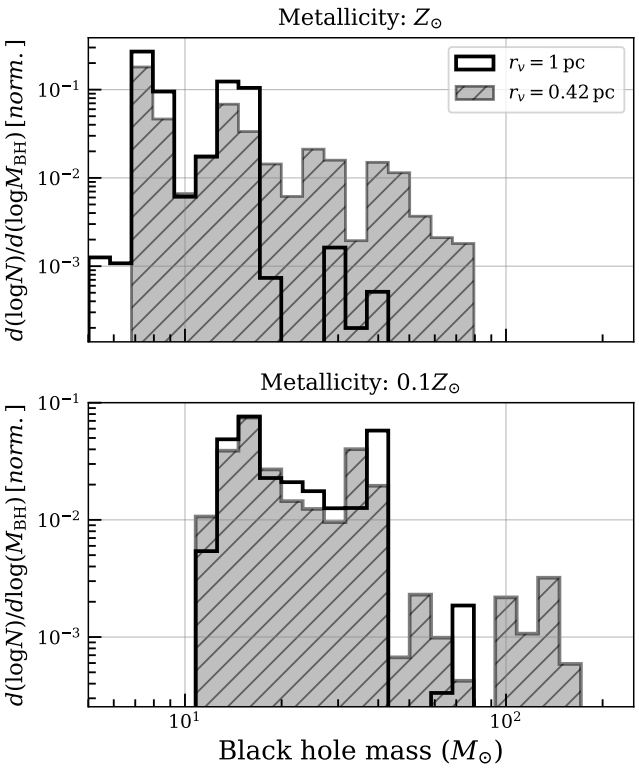

Figure 4. Normalized distribution of BH masses for all TDEs occurring in the various cluster models. In the top (bottom) panel, we show mass distributions for $Z_\odot$ ($0.1Z_\odot$) models. The solid black and hatched gray histograms show denote models adopting a constant $r_v = 1\,$pc and the $r_{\rm h} - M_{\rm cl}$ relation from Marks et al. (2012), respectively.

to lead to increased mass loss prior to stellar core collapse, which in turn is expected to reduce the mass of the BH ultimately formed (e.g., Vink et al. 2001; Fryer et al. 2012; Belczynski et al. 2016). For the $r_v = 1\,$pc models, we find median BH TDE masses of $13\,M_\odot$ and $27\,M_\odot$ for $Z_\odot$ and $0.1Z_\odot$, respectively.

We also see that, for a given metallicity, increasing the initial cluster density yields an extended tail in the upper part of the BH mass spectrum. This high-mass tail is populated by BHs formed through stellar collisions, which occur at an increased rate in higher density clusters. A number of recent analyses (Spera & Mapelli 2017; Di Carlo et al. 2019a,b; Kremer et al. 2020b) have demonstrated that dynamically-mediated stellar collisions occurring within the first roughly 5 Myr of cluster evolution (before formation of BHs) may lead to formation of massive stars that may ultimately collapse to form high-mass BHs. In particular, this process may permit formation of BHs with masses occupying the pair-instability mass gap from roughly $40 - 120\,M_\odot$ expected to arise through (pulsational) pair-instability supernovae (e.g., Belczynski et al. 2016; Woosley 2017; Spera & Mapelli 2017). Additionally, this process may be closely related to collisional runways which have been touted as a potential formation mechanism for intermediate-mass BHs (IMBHs) with masses in excess of roughly $100\,M_\odot$ (e.g., Portegies Zwart et al. 2004; Gürkan et al. 2006; Giersz et al. 2015; Mapelli 2016). Here, we adopt the same prescriptions implemented in Kremer et al. (2020b) to treat stellar collisions and the subsequent evolution of the collision products, as described in Section 2. We also assume the maximum BH mass formed through single-star evolution (i.e., unaffected by any dynamical processes) is $40.5\,M_\odot$, as determined by our (pulsational) pair-instability supernova treatment (see Belczynski et al. 2016, for detail).

In our $Z_\odot$ and $0.1Z_\odot$ models that adopt the Marks et al. (2012) $r_{\rm h}$ relation, we find roughly 10% of all TDEs have BH masses within the assumed pair-instability gap. In the $0.1Z_\odot$ models specifically, we find an additional 5% of TDEs occur with a BH mass in excess of $120\,M_\odot$ (the assumed upper limit to the pair-instability gap). These fractions are consistent with the rates of formation of massive BHs shown in previous studies of YSCs (Di Carlo et al. 2019a,b). Given the cosmological rates predicted in Section 3.3, these mass-gap and IMBH TDEs may constitute a non-negligible fraction of all TDEs occurring in YSCs. Furthermore, these TDEs may provide a potentially novel way to probe the formation of pair-instability gap BHs, similar to the recent LIGO/Virgo detection GW190521 (Abbott et al. 2020a,b).

Finally, comparing models `i,j,k` with models `e,f,g`, we see that lower metallicity clusters exhibit a moderate increase (a factor of roughly 1.4) in the total number of TDEs occurring through both single–single and binary–single encounters. This slight increase in the rate is anticipated: as shown in Equation 5, the TDE rate scales with the BH mass, $m_{\rm BH}$, through the influence of gravitational focusing and through tidal disruption radius calculation (Equation 1). Thus, we expect that metallicity leads to a moderate difference in the TDE rate for a given cluster mass.

4. ELECTROMAGNETIC SIGNATURES

In the previous section, we have shown that stellar-mass BH TDEs should be plentiful in YSCs. We now go on to examine possible electromagnetic signatures of these events, building upon previous work on this subject (e.g., Perets et al. 2016; Kremer et al. 2019d; Lopez et al. 2018; Fragione et al. 2019).

4.1. *Characteristic timescales and luminosities*

Following the disruption of a star of mass $m_\star$ and radius $R_\star$, the timescale, $t_{\rm fb}$ for (bound) orbiting material to fallback to the disruption point, $R_{\rm TD}$ is given by:

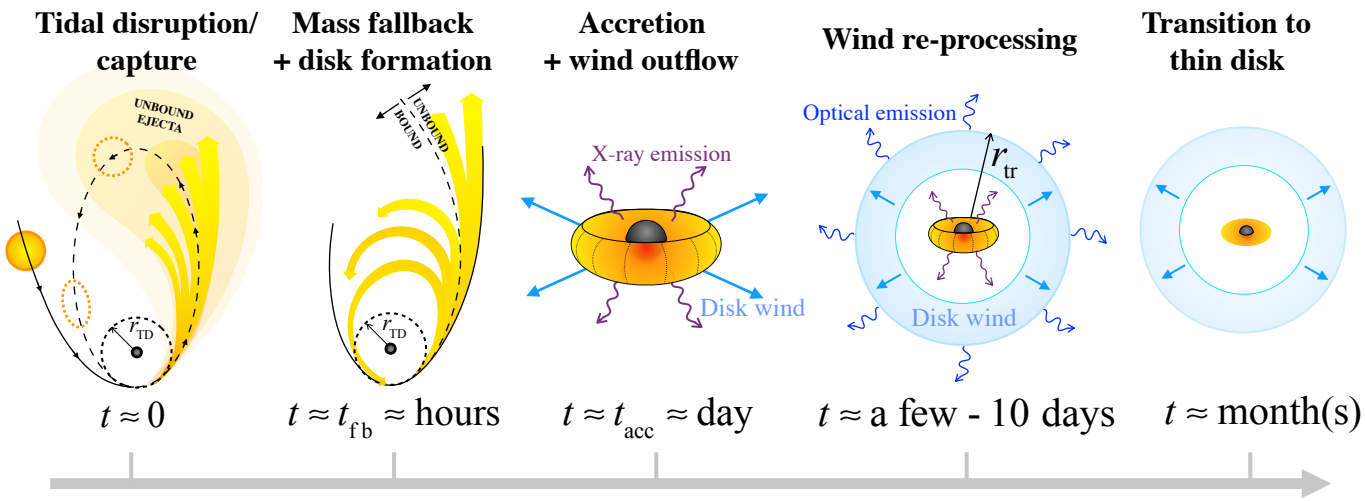

Figure 5. Schematic illustration of a stellar-mass BH tidal disruption event including disk formation and evolution in time. From left to right, we show: (1) Tidal disruption of the star, allowing for a possible initial partial disruption that unbinds a small fraction of stellar mass while the star is tidally captured into an elliptical orbit (see Section 4.3), (2) Fallback of bound material to pericenter, (3) Rise time for X-ray emission ($L_X \gtrsim 10^{44}\,{\rm erg\,s^{-1}}$; Equation 22) through viscous accretion onto the BH, (4) Re-processing of the X-ray emission by disk wind at the trapping radius leads to bright optical emission ($L_{\rm opt} \approx 10^{41} - 10^{44}\,{\rm erg\,s^{-1}}$), (5) Transition to thin disk and prompt drop in $\dot{M}$ and luminosity.

$$t_{\rm fb} = \frac{\pi R_{\rm TD}^3}{\sqrt{2Gm_{\rm BH}R_\star^3}} \approx 1.1\times10^4\,{\rm s}\left(\frac{m_\star}{M_\odot}\right)^{-1}\left(\frac{R_\star}{R_\odot}\right)^{3/2}\left(\frac{m_{\rm BH}}{10\,M_\odot}\right)^{1/2}. \quad (19)$$

(e.g., Perets et al. 2016).

For simplicity, we assume a disk is formed promptly at radius $r_d \simeq R_{\rm TD}$ and take $t_{\rm fb}$ as the characteristic timescale for disk formation. This is motivated by the fact that the orbits of the bound debris are only weakly eccentric. Once a disk is formed, the timescale for the debris to accrete is set by the viscous timescale (Shakura & Sunyaev 1973). For a thick disk, with disk height ratio $h = H/r_d$ (where H is the disk scale height), the viscous accretion timescale is

$$t_{\rm acc} \approx \left[h^2\alpha\Omega_{\rm K}(r_d)\right]^{-1} \approx 6\times10^4\,{\rm s}\left(\frac{h}{0.5}\right)^{-2}\left(\frac{\alpha}{0.1}\right)^{-1}\left(\frac{m_\star}{M_\odot}\right)^{-1/2}\left(\frac{R_\star}{R_\odot}\right)^{3/2} \quad (20)$$

Because the accretion time is larger than fallback time, we conclude the subsequent lightcurve evolution is viscosity-driven (i.e., determined by accretion timescale). This marks one key difference from supermassive BH TDEs, where $t_{\rm acc} \ll t_{\rm fb}$ and thus, the disk evolution is likely dominated by the fallback and the accretion rate is believed to follow the standard $t^{-5/3}$ power-law (e.g., Rees 1988; Phinney 1989; Evans & Kochanek 1989).

For viscosity-driven accretion, assuming roughly half of the stellar material is bound to the BH following the TDE (e.g., Rees 1988), the peak accretion rate can be approximated as

$$\dot{M}_p \approx \frac{m_\star/2}{t_{\rm acc}} \approx 2.6\times10^2\,M_\odot{\rm yr}^{-1}\left(\frac{h}{0.5}\right)^2\left(\frac{\alpha}{0.1}\right)\left(\frac{m_\star}{M_\odot}\right)^{3/2}\left(\frac{R_\star}{R_\odot}\right)^{-3/2} \quad (21)$$

The maximum possible luminosity is $L_{\rm max} \sim \epsilon\dot{M}_p c^2$, where $\epsilon \sim 0.1$ is the accretion efficiency near the innermost stable circular orbit (ISCO). This case corresponds to the most efficient energy release (possibly when a jet is formed), and we estimate $L_{\rm max} \sim 10^{48}\,{\rm erg\,s^{-1}}$ for typical TDE parameters. As pointed out in Perets et al. (2016), in this extreme case the TDE may power an ultra-long gamma ray burst (e.g., Gendre et al. 2013; Levan et al. 2014).

In the more widely accepted adiabatic inflow–outflow (ADIOS) model (Blandford & Begelman 1999), the mass inflow of a super-Eddington disk onto a BH is non-conservative and only a small fraction of the mass supplied at large radii is actually accreted. The accretion rate is expected to be reduced by factor $(10r_g/r_d)^s$, where $r_g = Gm_{\rm BH}/c^2$ is the BH gravitational radius, r_d is the disk radius, and the power-law index $s \in (0,1)$. The inner radius for the power-law scaling of the accretion rate is roughly at $10r_g$, slightly outside the ISCO. For the most pessimistic case of $s = 1$, we can estimate the accretion luminosity of the inner disk, a significant

fraction of which should be observable in the X-ray band for favorable viewing angles close to face-on,

$$L_{\rm min} \approx \epsilon\Big(\frac{10r_g}{r_d}\Big)\dot{M}_p c^2 \approx 1.5\times10^{44}\,{\rm erg\,s^{-1}}\left(\frac{m_\star}{M_\odot}\right)^{7/6}\left(\frac{m_{\rm BH}}{10\,M_\odot}\right)^{4/3}\left(\frac{R_\star}{R_\odot}\right)^{-5/2} \quad (22)$$

where we have once again assumed $h = 0.5$ and $\alpha = 0.1$. For $0 < s < 1$, we expect the accretion power to be somewhere in between 10^{44} and $10^{48}\,{\rm erg\,s^{-1}}$. For instance, based on numerical simulations of adiabatic accretion flows, Yuan et al. (2012) argued for $s \approx 0.5$ which corresponds to $L \sim 10^{46}\,{\rm erg\,s^{-1}}$.

At later time $t \gg t_{\rm acc}$, the disk radius expands as $r_d \propto t^{2/3}$ as a result of angular momentum conservation, the mass inflow rate drops as $\dot{M} \propto t^{-2(s+2)/3}$, and the BH accretion rate drops as $\dot{M}_{\rm BH} \propto t^{-4(s+1)/3}$ (e.g., Kumar et al. 2008). Thus, the late-time X-ray lightcurve is a power-law between $L_X \propto t^{-4/3}$ and $t^{-8/3}$.

The majority of the mass inflow is lost from the disk in the form of a radiatively driven wind. The energy generated by accretion in the inner disk is expected to be reprocessed by this wind and released at the photon trapping radius, $r_{\rm tr}$, where the radiative diffusion time equals to the expansion time (typically occurring a few to 10 days after the TDE; Kremer et al. 2019d). A rough estimate for the trapping radius is

$$r_{\rm tr} \approx \min\left(v_{\rm w}t, \frac{\dot{M}(t)\kappa}{4\pi c}\right) \approx 10^{15}{\rm cm}\,\min\left(\frac{v_{\rm w}}{10^9\,{\rm cm\,s^{-1}}}\frac{t}{10^6\,{\rm s}}, \frac{\dot{M}(t)}{17M_\odot\,{\rm yr^{-1}}}\right), \quad (23)$$

where $v_{\rm w} \approx 10^9\,{\rm cm\,s^{-1}}$ is the typical wind speed (Kremer et al. 2019d) and $\kappa = 0.34\,{\rm cm^2\,g^{-1}}$ is electron scattering opacity.

For a detailed discussion of the radiation hydrodynamics of the accretion disk and wind, we direct the reader to Kremer et al. (2019d); Piro & Lu (2020) and references therein. Here, we summarize the key points. As a result of adiabatic loss, the emerging luminosity is smaller than the accretion luminosity by a factor of $(r_d/r_{\rm tr})^{2/3} \sim 10^{-2}$ for $r_{\rm tr} \sim 10^{15}\,{\rm cm}$ and $r_d \sim 10^{12}\,{\rm cm}$ roughly at $t \sim 10\,{\rm days}$. Kremer et al. (2019d) considered $s \in (0.2, 0.8)$ and found the peak bolometric luminosity to be in the range $10^{41} - 10^{44}\,{\rm erg\,s^{-1}}$ (depending also upon the assumed stellar parameters, such as masses) and the spectrum to be in the optical/UV, for typical stellar-mass BH TDEs.

This optical emission is expected to last roughly $10-100$ days until the mass inflow rate drops below roughly $(r_d/r_g)L_{\rm Edd}/c^2$, at which point the disk is expected to transition to a geometrically thin state and the accretion rate may drop by many orders of magnitude (Shen & Matzner 2014).

In Figure 5, we summarize the key evolutionary features of the first roughly 100 days following the tidal disruption.

4.2. *Comparison to Fast Blue Optical Transients*

Recent high-cadence surveys have uncovered a growing number of fast-evolving transients with a wide range of observed properties. One class of particular interest is the Fast Blue Optical Transients (FBOTs; Drout et al. 2014), also known as Fast Evolving Luminous Transients (FELTs; Rest et al. 2018). Although a clear understanding of FBOTs remains elusive, this class of transients is generally defined by rise times (of order one to a few days) and peak luminosities (roughly $10^{41}-10^{44}\,{\rm erg\,s^{-1}}$) that are too fast and too luminous to be explained by the radioactive decay of ^{56}Ni. The majority of FBOTs are found in star-forming galaxies of roughly solar metallicity. Furthermore, the explosion sites span a range of off-sets from the galaxy centers, most closely resembling the off-set distribution of core-collapse supernovae (e.g., Drout et al. 2014).

The majority of FBOTs have been identified via archival searches of various optical surveys including the Pan-STARRS1 Medium Deep Survey (PS1-MDS; Drout et al. 2014), the Dark Energy Survey (Pursiainen et al. 2018), Kepler (Rest et al. 2018), the Supernova Legacy Survey (Arcavi et al. 2016), and the Zwicky Transient Facility (ZTF; Ho et al. 2020). In addition to the archival searches, a handful of FBOTs have been discovered while still active, notably AT2018cow (Margutti et al. 2019), ZTF18abvkwla (Ho et al. 2020), and CSS161010 (Coppejans et al. 2020). Subsequent X-ray/radio follow-up of these particular events has provided various insights into the possible progenitors of FBOTs not possible from optical observations alone.

Various analyses have computed volumetric rates of transients similar to FBOTs, with estimates ranging from roughly $100\,{\rm Gpc^{-3}\,yr^{-1}}$ to more than $1000\,{\rm Gpc^{-3}\,yr^{-1}}$ in the local universe (e.g., Drout et al. 2014; Pursiainen et al. 2018; Ho et al. 2020; Coppejans et al. 2020). Although the precise rate remains uncertain, the general consensus appears to be that FBOTs are roughly two to three orders of magnitude rarer than standard core-collapse supernovae (e.g., Botticella et al. 2008).

The specific origin of FBOTs remains unknown with a number of channels having been proposed including TDEs by IMBHs (Perley et al. 2019), massive star collapse and BH formation (Quataert et al. 2019), electron capture collapse following a white dwarf merger (Lyutikov & Toonen 2019), and magnetar formation (Margutti et al. 2019). Additionally, Piro & Lu (2020) pointed out that many FBOT features (specifically in the case of AT2018cow) show similarities to what would

Table 3. Comparison of key features of stellar-mass BH TDEs and FBOTs

	Stellar-mass BH TDEs	FBOTs
Peak optical luminosity [erg s^{-1}]	$\approx 10^{41} - 10^{44}$	**Overall:** $\approx 10^{41} - 10^{44}$ (Drout et al. 2014; Pursiainen et al. 2018) *AT2018cow:* $\approx 4 \times 10^{44}$ (Margutti et al. 2019) *ZTF18abvkwla:* $\approx 10^{44}$ (Ho et al. 2019)
Optical rise time [days]	$\approx$ a few $-$ 10	**Overall:** $\lesssim 5$ (Drout et al. 2014; Pursiainen et al. 2018) *AT2018cow:* 1.43 ± 0.08 (Prentice et al. 2018; Perley et al. 2019) *ZTF18abvkwla:* 1.83 ± 0.05 (Ho et al. 2019)
Fade time [days]	$\approx$ a few	**Overall:** $\sim$ a few $-$ 10 (Drout et al. 2014; Pursiainen et al. 2018) *AT2018cow:* 1.95 ± 0.06 (Prentice et al. 2018; Perley et al. 2019) *ZTF18abvkwla:* 3.12 ± 0.22 (Ho et al. 2019)
X-ray luminosity [erg s^{-1}]	(assuming unabsorbed)	(Observed values are for $0.3 - 10$ keV)
≈ 1 d after peak	$\approx 10^{43} - 10^{47}$	*AT2018cow:* $\approx 10^{43}$ (Margutti et al. 2019)
≈ 10 d after peak	$\approx 10^{41} - 10^{46}$	*AT2018cow:* $\approx 5 \times 10^{42}$ (Margutti et al. 2019)
≈ 100 d after peak	$\approx 10^{38} - 10^{45}$	*AT2018cow:* $\approx 10^{40}$ (Margutti et al. 2019) *CSS161010:* $\approx 5 \times 10^{39}$ (Coppejans et al. 2020)
Volumetric rate [Gpc^{-3} yr^{-1}]	$30 - 300$	< 560 (For $M_g < -20$; Ho et al. 2020) $700 - 1400$ (For $M_g < -19$; Coppejans et al. 2020) $\gtrsim 1000$ (For $-15.8 < M_g < -22.2$; Pursiainen et al. 2018)
CSM density [cm^{-3}]	$\approx 10^2 - 10^5$ (?) (Section 4.3)	*AT2018cow:* $\approx 10^5 - 10^6$ ($t = 22$d, $v \approx 0.1c$; Ho et al. 2019) *ZTF18abvkwla:* $\approx 200 - 2000$ ($t = 81$d, $v \approx 0.4c$; Ho et al. 2020) *CSS161010:* $\approx 20 - 300$ ($t = 99$d, $v \approx 0.6c$; Coppejans et al. 2020)

NOTE—Summary of key features of stellar-mass BH TDEs alongside inferred FBOT properties from various references in the literature. For optical luminosity and rise time, we show "Overall" properties of the full FBOT population. For other features we list only observations from specific FBOTs, namely AT2018cow, CSS161010, and ZTF18abvkwla. The upper and lower bounds for theoretical X-ray luminosities of TDEs assume $s = 0$ and $s = 1$ power-law indices for the accretion rate, assuming no absorption; see Section 4.1. We show inferred CSM densities for a single epoch of radio observation for each observed FBOT. The observation time and inferred shock velocity is listed for each event; see references for further detail.

be expected for a wind-reprocessed transient, regardless of the specific central engine.

Here, we propose stellar-mass BH TDEs as another possible FBOT progenitor. The rise times and peak optical luminosities predicted for these TDEs (Section 4.1 and Kremer et al. 2019d) occupy the same region of parameter space expected for FBOTs, as does the estimated X-ray luminosity. If these TDEs occur in high-metallicity young stellar clusters (expected to be a dominant site for star formation; Lada & Lada 2003), the host galaxy type and off-set distribution for observed FBOTs may also be recovered. Furthermore, the rate we predict for stellar-mass BH TDEs in YSCs (up to roughly 300 Gpc^{-1} yr^{-1} in the local universe) is comparable to the observationally-inferred FBOT rates. In light of these similarities, stellar-mass BH TDEs that occur in YSCs may *in principle* be a viable progentor for FBOT-like transients.

In Table 3, we summarize for comparison the key features of both FBOTs and stellar-mass BH TDEs.

4.3. *Radio emission and inferred external medium*

Although it remains to be determined whether bright radio emission is a defining feature of the FBOT class broadly, radio emission is observed for the AT2018cow, ZTF18abvkwla, and CSS161010 events. Thus, the statement that stellar-mass BH TDEs are viable FBOT progenitors warrants a discussion of this topic.

The observed radio emission from the above three events is consistent with self-absorbed synchrotron (SSA) radiation produced from an external shock generated as the ejecta interacts with a dense external medium (e.g., Margutti et al. 2019). Following the standard framework for self-absorbed synchrotron emission from SNe (e.g., Chevalier 1998), Margutti et al. (2019); Ho et al. (2020); Coppejans et al. (2020) inferred circumstellar medium (CSM) densities ranging from roughly

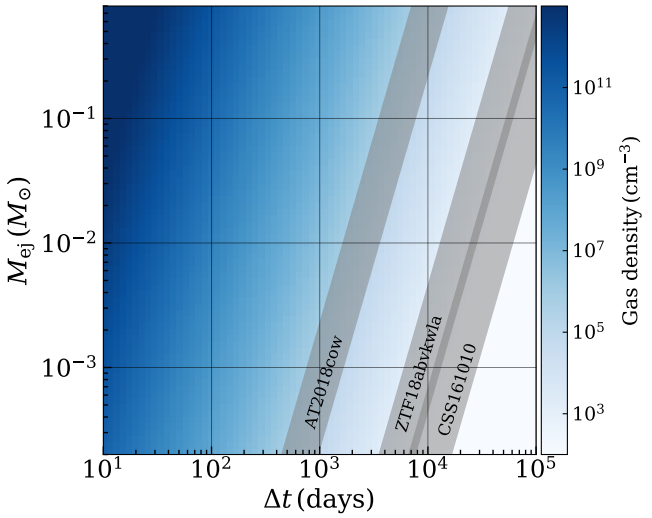

Figure 6. Local gas density predicted from expansion of ejecta associated with a partial tidal disruption occurring a time Δt before the main TDE (Equation 24). We show as gray bands the ranges of constant density inferred for AT2017cow (Ho et al. 2019), ZTF18abvkwla (Ho et al. 2020), and CSS161010 (Coppejans et al. 2020) from radio observations 22, 81, and 99 days after each respective explosion.

$10 - 10^6\,{\rm cm}^{-3}$ for AT2017cow, ZTF18abvkwla, and CSS161010, respectively, for various observation epochs and for a range of microphysics assumptions. We summarize the inferred density estimates in Table 3. As discussed in Margutti et al. (2019) in the context of AT2018cow, the high-density CSM inferred from radio observations may pose difficulties for a TDE interpretation of FBOTs. The discussion in Margutti et al. (2019) concerned specifically IMBH TDEs (e.g., Perley et al. 2019), however similar arguments may apply in the case of stellar-mass BH TDEs.

Here, we describe two speculative yet plausible scenarios applying to stellar-mass BH TDEs in YSCs which may yield a CSM with density comparable to that inferred for previous FBOTs:

• *Wind mass loss from asymptotic giant branch stars:* After roughly 30 Myr, stars with zero-age main sequence masses in the range roughly $4 - 10\,M_\odot$ begin to evolve through the asymptotic giant branch (AGB) phase and begin to lose mass through stellar winds. Due to the low velocity expected for AGB winds ($\sim 10 - 30\,{\rm km/s}$; Loup et al. 1993), the wind ejecta may be retained in the host cluster, potentially leading to a reservoir of gas (e.g., Bastian & Lardo 2018). Indeed, previous work has argued that AGB winds may potentially supply sufficient material to give rise to a second population of stars in the cluster (e.g., D'Ercole et al. 2008). This gas reservoir is likely retained in its host cluster for roughly $100 - 200\,{\rm Myr}$, until the first Type Ia supernovae occur, which will likely clear the cluster of any remaining gas (e.g., Bastian & Lardo 2018). Nonetheless, this potentially provides a sufficient window of time for outflows from stellar-mass BH TDEs to interact with this gaseous material.

For a standard Kroupa (2001) IMF, roughly 10% of a cluster's total mass lies within this mass range $4-10\,M_\odot$. Assuming that $\sim$ 80 % of the stellar mass of these stars are lost to AGB winds (e.g., van den Hoek & Groenewegen 1997) and assuming for simplicity the gas spread uniformly within the cluster's half-mass radius, $r_{\rm h} \approx 1\,{\rm pc}$, we can estimate a gas density of roughly $n \approx 80 - 8000\,M_\odot\,{\rm pc}^{-3} \approx 10^3 - 10^5\,{\rm cm}^{-3}$, for clusters of masses of $10^3 - 10^5\,M_\odot$. For $r_{\rm h} \approx 0.5\,{\rm pc}$, as predicted in Marks et al. (2012), the density may reach as high as $10^6\,{\rm cm}^{-3}$. Thus, although various details are highly uncertain, AGB winds could *plausibly* produce a sufficiently dense CSM[3].

• *Mass outflow from partial tidal disruption:* If prior to its tidal disruption, a main sequence star is tidally captured by a BH, such that a small amount of orbital energy is deposited into the star (e.g., Fabian et al. 1975, see left-most panel of Figure 5 for illustration), a small amount of debris may be unbound from the star. This may occur either through partial stripping by the BH at the first pericenter passage or during subsequent pericenter passages if the star's envelope expands due to energy injected through the tidal encounter. The detailed hydrodynamics of this process are well beyond the scope of this paper. However, we can speculate that, if this unbound ejecta of mass $M_{\rm ej}$ and velocity, $v_{\rm ej} \approx 10^3 {\rm km\,s}^{-1}$ (slightly larger than the escape velocity of the star) expands homologously with a constant density for a time Δt before the main disruption event, a gaseous medium may form in the local vicinity of the BH. A simple estimate yields the following scaling for the ejecta density:

$$n_{\rm ej} \approx 10^5\,{\rm cm}^{-3} \left(\frac{M_{\rm ej}}{10^{-2}\,M_\odot}\right)\left(\frac{v_{\rm ej}}{10^3\,{\rm km/s}}\right)^{-3}\left(\frac{\Delta t}{10\,{\rm yr}}\right)^{-3}. \quad (24)$$

In Figure 6, we show the gas density expected from Equation 24 for various values of $M_{\rm ej}$ and Δt (the assumed time elapsed between partial disruption and complete disruption of the star). For reference, the gray bands mark ranges of constant density inferred from radio observations of AT2018cow (Ho et al. 2019), ZTF18abvkwla (Ho et al. 2020), and CSS161010 (Coppejans et al. 2020) 22, 81, and 99 days after explosion, respectively. Also see Table 3 for details. Again, we emphasize that this process is highly speculative, but note that in principle (i.e., assuming reasonable values of $M_{\rm ej} \sim 10^{-3} - 10^{-2} M_\odot$ and $\Delta t \sim$ years), this may produce a CSM with density comparable to that inferred

[3] The radial density profile in this case is roughly constant above the Bondi radius $r_{\rm B} \sim GM/\sigma_v^2$ and a power-law $n \propto r^{-3/2}$ below $r_{\rm B}$.

from observed radio emission of FBOTs. More detailed hydrodynamic models of disruption and outflow of unbound ejecta are required to calculate the radial density profile and test this possibility.

For radio-bright FBOTs, the CSM density profiles are constrained by the evolution of the radio spectral energy distribution (SED). In the simplest spherically symmetric model, the peak frequency $\nu_{\rm p}$ and the peak specific luminosity $L_{\nu_{\rm p}}$ are such that the synchrotron self-absorption optical depth is order unity. This means that $L_{\nu_p} \sim 4\pi^2 r^2 2\nu_{\rm p}^2 \gamma_{\rm p} m_e \sim N(\gamma_{\rm p}) e^3 B / m_e c^2$ (Kumar & Zhang 2015), where r is the shock radius, $\gamma_{\rm p} = \sqrt{2\pi m_e c \nu_{\rm p}/eB}$ is the Lorentz factor of the electrons emitting near $\nu_{\rm p}$, B is the magnetic field strength in the emitting region, e is the fundamental charge unit, and $N(\gamma_{\rm p})$ is the number of radiating electrons with Lorentz factors near $\gamma_{\rm p}$. Detailed modeling of the electron Lorentz factor distribution is needed to fit the observed SED to obtain $\nu_{\rm p}$ and $L_{\nu_{\rm p}}$, which in turn involves considerable uncertainties regarding particle acceleration and cooling. A simpler approach is to notice that, for a power-law Lorentz factor distribution, the SED below the peak frequency is $L_{\nu<\nu_{\rm p}} \simeq L_{\nu_{\rm p}} (\nu/\nu_{\rm p})^{5/2} \propto \nu^{5/2} r^2 B^{-1/2}$. If the magnetic fields take a constant fraction of the thermal energy of the shocked region, then we have $B \propto n^{1/2} v$ for CSM density n and shock velocity v. For a power-law CSM profile $n \propto r^{-q}$ and $r \sim vt$, we obtain $L_{\nu<\nu_{\rm p}} \propto \nu^{5/2} v^{3/2+q/4} t^{2+q/4}$. For instance, for AT2018cow, the flux at $\nu = 34\,{\rm GHz}$ (which is much below $\nu_{\rm p}$) evolves close to a power-law $F_{\nu=34\,{\rm GHz}} \propto t^2$ in the first month (Ho et al. 2019), and this indicates that the density profile is rather shallow ($q \lesssim 2$) and that the velocity is roughly constant.[4]

We have limited our discussion here to simple order-of-magnitude estimates of CSM densities and do not consider whether the aforementioned scenarios associated with TDEs may reproduce density profiles consistent with detailed interpretation of the observations. From the rough estimates considered here, it appears the density profiles of observed FBOTs are not sufficiently well constrained to rule out the stellar-mass BH TDE scenario. More detailed examination of this question in future studies may provide further insight into the comparison of stellar-mass BH TDEs to observed FBOTs.

5. CONCLUSIONS & DISCUSSION

5.1. *Summary*

We summarize here the main findings of this work:

1. Using a suite of roughly 3000 N-body simulations, we have explored the rates and properties of stellar-mass BH TDEs in YSCs. We derived TDE rates as a function of cluster mass and showed that the rates derived from the models agree closely with rates derived from simple analytic estimates.

2. Using the rate scalings derived from our models and integrating over the full cluster mass function, we predict these TDEs occur at a rate of roughly $30 - 300\,{\rm Gpc^{-3}\,yr^{-1}}$ in the local universe. The range in this estimate is determined primarily by the assumptions made concerning initial cluster densities (e.g., Portegies Zwart et al. 2010; Marks et al. 2012). Overall, we find TDEs occur a factor of a few to 10 times more frequently in binary-mediated dynamical encounters compared to single–single encounters.

3. In YSCs of roughly solar metallicity, we predict a median BH mass of roughly $10\,M_\odot$. In lower-metallicity ($Z \lesssim 0.1 Z_\odot$) clusters that may have formed at higher redshift, we predict a median mass of roughly $30\,M_\odot$. This difference is primarily a result of the metallicity-dependent stellar wind mass loss (Vink et al. 2001).

4. We showed that stellar-mass BH TDEs exhibit the following key features: (i) rise times of roughly a day driven by the viscous accretion timescale, (ii) peak X-ray luminosities of roughly $10^{44} - 10^{48}\,{\rm erg\,s^{-1}}$, and (iii) optical luminosities of up to roughly $10^{44}\,{\rm erg\,s^{-1}}$ produced by re-processing of X-rays by a disk wind on a timescale of a few to 10 days after the TDE. On the basis of all of these features, combined with the estimated TDE rates and host-galaxy properties, we propose stellar-mass BH TDEs as a viable progenitor for the FBOT class of transients (e.g., Drout et al. 2014; Margutti et al. 2019; Ho et al. 2020; Coppejans et al. 2020).

5. Radio emission has been observed for three FBOT events. Depending upon assumptions made regarding AGB wind mass loss and/or mass ejecta from partial tidal disruption during a tidal capture, the presence of a CGM sufficiently dense to produce the observed radio emission may be plausible. However, more detailed models are necessary to test this possibility.

5.2. *Discussion & Future Work*

Although the event rates inferred from FBOT observations are uncertain and vary between different analyses, in general, the observed FBOT rate appears higher than the stellar-mass BH TDE rate estimated from our models by a small factor (see Table 3). However, there are several reasons why our estimated rate may underestimate the true TDE rate, possibly explaining this discrepancy:

[4] The temporal evolution of $F_{\nu=34\,{\rm GHz}}$ becomes less sensitive to q as it gets smaller, thus this simple analysis produces only an upper limit for q, as opposed to a more precise measurement.

First, in this study, we have assumed zero primordial binaries. BH binaries were allowed to form exclusively through three-body formation (see Section 2). Although a detailed understanding of primordial binary fractions in YSCs remains elusive, binary fractions observed for stars in the Galactic field (e.g., Sana et al. 2012) suggest high binary fractions may be plausible. Stellar binaries are known to increase the rates of dynamical collisions and TDEs (e.g., Fregeau & Rasio 2007). In this case, our predicted TDE rates may in fact be a lower limit. Follow-up studies may examine more expansively the potential role of primordial binaries.

Second, as discussed briefly in Section 4, a fraction of TDEs may occur through tidal capture where the main sequence star may undergo multiple passages before ultimately being disrupted. As discussed in e.g., Fabian et al. (1975), the cross section for tidal capture may be a factor of roughly a few times larger than that for tidal disruption. If the fate of the majority of tidal captures is a TDE, the total TDE rate may be higher than that estimated here by a factor of a few.

In Section 3.4, we showed that, depending on the assumed initial virial radius and cluster metallicity, IMBHs with masses in excess of $100\,M_\odot$ may form in YSCs through stellar collisions (see also Di Carlo et al. 2019a; Kremer et al. 2020b) and ultimately undergo TDEs. The topic of TDEs by IMBHs in stellar clusters has been examined at length (e.g., Rosswog et al. 2009; MacLeod et al. 2014, 2016; Fragione et al. 2020). We have focused in this study on the more common (by a factor of roughly 10:1 or higher in our models) stellar-mass BH TDE. However, IMBH TDEs likely lead to several notable differences. For example, for sufficiently massive IMBHs, the TDEs will transition from viscosity driven to fallback driven, thus becoming qualitatively more similar to a supermassive BH TDE (e.g., Rees 1988). We reserve for future work a more careful examination of the properties and observational signatures of TDEs by IMBHs.

We have used here the `CMC` code to model the evolution of YSCs. The Monte Carlo-based approach used in `CMC` allows us to model large populations of clusters at low computational expense compared to direct N-body models (e.g., Pattabiraman et al. 2013; Rodriguez et al. 2016). However, unlike massive globular clusters, the relatively low-mass YSCs studied here can also be studied efficiently with direct N-body models (e.g., Di Carlo et al. 2019a; Banerjee 2017). Future work may examine the topic of TDEs using direct N-body models which would allow detailed examination of several regimes Monte Carlo simulations like `CMC` are ill-equipped to study. For example, examination of the final stage of cluster's life as it dissolves on a dynamical timescale through its tidal boundary and examination of clusters that contain massive IMBHs (as discussed in the previous paragraph) that may affect the overall cluster and TDE dynamics.

Finally, unlike supermassive BH TDEs which have been studied extensively with hydrodynamic simulations, the stellar-mass BH regime has been little explored, with a few exceptions (Perets et al. 2016; Lopez et al. 2018). Ultimately, hydrodynamic models are necessary to understand many of the detailed features (both theoretical and observational) of these events. For example, in the analytic estimates in Section 4, we considered only those interactions near the tidal disruption boundary, $r_{\rm TD}$, of the star. However, given that the interaction cross section scales linearly with stellar radius (Equation 4), a reasonable fraction of such BH–star encounters may actually occur in the direct collision regime, where $r_p < R_\star$ (e.g., Fryer & Woosley 1998; Hansen & Murali 1998). Although this subclass of "head on" encounters is unlikely to affect our rate predictions by more than a small factor, these physical collisions may produce a subclass of unique transients. For instance, a direct collision may lead to prompt accretion (i.e., $t_{\rm fb} \approx 0$) onto the BH which, among other possible consequences, may make the effects of feedback critical on the subsequent evolution, if indeed a disk forms at all. On the other hand, as mentioned briefly in Section 4, even more distant encounters ($r_p > r_{\rm TD}$) may lead to tidal capture, possibly resulting in multiple passages that each partially strip the star (e.g., Fabian et al. 1975; Ivanova et al. 2017), again potentially producing EM signatures unique from those presented in the classic TDE regime discussed in Section 4. More careful treatment of the various regimes of these BH–star interactions, ideally with hydrodynamic models, is necessary to explore the potentially broad range of outcomes of these events in greater detail. Specifically, this detail will be crucial to determine the fraction of these events that may exhibit similarities to FBOTs versus other possible transients with their own unique properties.

ACKNOWLEDGMENTS

We thank Carl Rodriguez for useful discussion. K.K. is supported by an NSF Astronomy and Astrophysics Postdoctoral Fellowship under award AST-2001751. W.L. is supported by the David and Ellen Lee Fellowship at Caltech. S.C. acknowledges support of the Department of Atomic Energy, Government of India, under project no. 12-R&D-TFR-5.02-0200. F.A.R. and C.S.Y. acknowledge support from NSF Grant AST-1716762 at Northwestern University.

REFERENCES

Abbott, R., Abbott, T. D., Abraham, S., et al. 2020a, The Astrophysical Journal, 900, L13, doi: 10.3847/2041-8213/aba493

—. 2020b, Phys. Rev. Lett., 125, 101102, doi: 10.1103/PhysRevLett.125.101102

Antonini, F., & Gieles, M. 2019, arXiv e-prints, arXiv:1906.11855. https://arxiv.org/abs/1906.11855
Arca Sedda, M., Askar, A., & Giersz, M. 2018, MNRAS, 479, 4652, doi: 10.1093/mnras/sty1859
Arcavi, I., Wolf, W. M., Howell, D. A., et al. 2016, ApJ, 819, 35, doi: 10.3847/0004-637X/819/1/35
Askar, A., Arca Sedda, M., & Giersz, M. 2018, MNRAS, 478, 1844, doi: 10.1093/mnras/sty1186
Banerjee, S. 2017, MNRAS, 467, 524, doi: 10.1093/mnras/stw3392
—. 2018, MNRAS, 481, 5123, doi: 10.1093/mnras/sty2608
—. 2020, arXiv e-prints, arXiv:2004.07382. https://arxiv.org/abs/2004.07382
Bastian, N., & Lardo, C. 2018, ARA&A, 56, 83, doi: 10.1146/annurev-astro-081817-051839
Bate, M. R., Bonnell, I. A., & Bromm, V. 2003, MNRAS, 339, 577, doi: 10.1046/j.1365-8711.2003.06210.x
Belczynski, K., Heger, A., Gladysz, W., et al. 2016, Astronomy & Astrophysics, 594, A97, doi: 10.1051/0004-6361/201628980
Bellm, E. C., Kulkarni, S. R., Graham, M. J., et al. 2019, PASP, 131, 018002, doi: 10.1088/1538-3873/aaecbe
Binney, J., & Tremaine, S. 1987, Galactic dynamics
Blandford, R. D., & Begelman, M. C. 1999, MNRAS, 303, L1, doi: 10.1046/j.1365-8711.1999.02358.x
Botticella, M. T., Riello, M., Cappellaro, E., et al. 2008, A&A, 479, 49, doi: 10.1051/0004-6361:20078011
Breen, P. G., & Heggie, D. C. 2013, MNRAS, 432, 2779, doi: 10.1093/mnras/stt628
Carpenter, J. M. 2000, AJ, 120, 3139, doi: 10.1086/316845
Chambers, K. C., Magnier, E. A., Metcalfe, N., et al. 2016, arXiv e-prints, arXiv:1612.05560. https://arxiv.org/abs/1612.05560
Chatterjee, S., Rodriguez, C. L., & Rasio, F. A. 2017, ApJ, 834, 68, doi: 10.3847/1538-4357/834/1/68
Chevalier, R. A. 1998, ApJ, 499, 810, doi: 10.1086/305676
Chomiuk, L., Strader, J., Maccarone, T. J., et al. 2013, ApJ, 777, 69, doi: 10.1088/0004-637X/777/1/69
Coppejans, D. L., Margutti, R., Terreran, G., et al. 2020, ApJL, 895, L23, doi: 10.3847/2041-8213/ab8cc7
Coughlin, E. R., Armitage, P. J., Nixon, C., & Begelman, M. C. 2017, MNRAS, 465, 3840, doi: 10.1093/mnras/stw2913
Darbha, S., Coughlin, E. R., Kasen, D., & Quataert, E. 2018, MNRAS, 477, 4009, doi: 10.1093/mnras/sty822
D'Ercole, A., Vesperini, E., D'Antona, F., McMillan, S. L. W., & Recchi, S. 2008, MNRAS, 391, 825, doi: 10.1111/j.1365-2966.2008.13915.x
Di Carlo, U. N., Giacobbo, N., Mapelli, M., et al. 2019a, arXiv e-prints. https://arxiv.org/abs/1901.00863
Di Carlo, U. N., Mapelli, M., Bouffanais, Y., et al. 2019b, arXiv e-prints, arXiv:1911.01434. https://arxiv.org/abs/1911.01434
Drout, M. R., Chornock, R., Soderberg, A. M., et al. 2014, ApJ, 794, 23, doi: 10.1088/0004-637X/794/1/23
Evans, C. R., & Kochanek, C. S. 1989, ApJL, 346, L13, doi: 10.1086/185567
Fabian, A. C., Pringle, J. E., & Rees, M. J. 1975, MNRAS, 172, 15p, doi: 10.1093/mnras/172.1.15P
Fragione, G., Leigh, N. W. C., Perna, R., & Kocsis, B. 2019, MNRAS, 489, 727, doi: 10.1093/mnras/stz2213
Fragione, G., Perna, R., & Loeb, A. 2020, arXiv e-prints, arXiv:2006.14632. https://arxiv.org/abs/2006.14632
Fregeau, J. M., & Rasio, F. A. 2007, ApJ, 658, 1047, doi: 10.1086/511809
Fryer, C. L., Belczynski, K., Wiktorowicz, G., et al. 2012, ApJ, 749, 91, doi: 10.1088/0004-637X/749/1/91
Fryer, C. L., & Woosley, S. E. 1998, ApJL, 502, L9, doi: 10.1086/311493
Gendre, B., Stratta, G., Atteia, J. L., et al. 2013, ApJ, 766, 30, doi: 10.1088/0004-637X/766/1/30
Gieles, M., Portegies Zwart, S. F., Baumgardt, H., et al. 2006, MNRAS, 371, 793, doi: 10.1111/j.1365-2966.2006.10711.x
Giersz, M., Askar, A., Wang, L., et al. 2019, MNRAS, 487, 2412, doi: 10.1093/mnras/stz1460
Giersz, M., Leigh, N., Hypki, A., Lützgendorf, N., & Askar, A. 2015, MNRAS, 454, 3150, doi: 10.1093/mnras/stv2162
Giesers, B., Dreizler, S., Husser, T.-O., et al. 2018, MNRAS, 475, L15, doi: 10.1093/mnrasl/slx203
Giesers, B., Kamann, S., Dreizler, S., et al. 2019, arXiv e-prints, arXiv:1909.04050. https://arxiv.org/abs/1909.04050
Giesler, M., Clausen, D., & Ott, C. D. 2018, MNRAS, 477, 1853, doi: 10.1093/mnras/sty659
Gnedin, O. Y., Lee, H. M., & Ostriker, J. P. 1999, ApJ, 522, 935, doi: 10.1086/307659
Gürkan, M. A., Fregeau, J. M., & Rasio, F. A. 2006, ApJL, 640, L39, doi: 10.1086/503295
Hansen, B. M. S., & Murali, C. 1998, ApJL, 505, L15, doi: 10.1086/311602
Heggie, D., & Hut, P. 2003, The Gravitational Million-Body Problem: A Multidisciplinary Approach to Star Cluster Dynamics
Ho, A. Y. Q., Phinney, E. S., Ravi, V., et al. 2019, ApJ, 871, 73, doi: 10.3847/1538-4357/aaf473
Ho, A. Y. Q., Perley, D. A., Kulkarni, S. R., et al. 2020, ApJ, 895, 49, doi: 10.3847/1538-4357/ab8bcf
Hopkins, A. M., & Beacom, J. F. 2006, ApJ, 651, 142, doi: 10.1086/506610

Hurley, J. R., Pols, O. R., & Tout, C. A. 2000, MNRAS, 315, 543, doi: 10.1046/j.1365-8711.2000.03426.x

Hurley, J. R., Tout, C. A., & Pols, O. R. 2002, MNRAS, 329, 897, doi: 10.1046/j.1365-8711.2002.05038.x

Ivanova, N., Chaichenets, S., Fregeau, J., et al. 2010, ApJ, 717, 948, doi: 10.1088/0004-637X/717/2/948

Ivanova, N., da Rocha, C. A., Van, K. X., & Nandez, J. L. A. 2017, ApJL, 843, L30, doi: 10.3847/2041-8213/aa7b76

Joshi, K. J., Rasio, F. A., Zwart, S. P., & Portegies Zwart, S. 2000, The Astrophysical Journal, 540, 969, doi: 10.1086/309350

King, I. 1962, AJ, 67, 471, doi: 10.1086/108756

Kochanek, C. S., Shappee, B. J., Stanek, K. Z., et al. 2017, PASP, 129, 104502, doi: 10.1088/1538-3873/aa80d9

Kremer, K., Chatterjee, S., Rodriguez, C. L., & Rasio, F. A. 2018a, ApJ, 852, 29, doi: 10.3847/1538-4357/aa99df

Kremer, K., Chatterjee, S., Ye, C. S., Rodriguez, C. L., & Rasio, F. A. 2019a, ApJ, 871, 38, doi: 10.3847/1538-4357/aaf646

Kremer, K., D'Orazio, D. J., Samsing, J., Chatterjee, S., & Rasio, F. A. 2019b, ApJ, 885, 2, doi: 10.3847/1538-4357/ab44d1

—. 2019c, ApJ, 885, 2, doi: 10.3847/1538-4357/ab44d1

Kremer, K., Lu, W., Rodriguez, C. L., Lachat, M., & Rasio, F. 2019d, arXiv e-prints. https://arxiv.org/abs/1904.06353

Kremer, K., Ye, C. S., Chatterjee, S., Rodriguez, C. L., & Rasio, F. A. 2018b, ApJL, 855, L15, doi: 10.3847/2041-8213/aab26c

Kremer, K., Ye, C. S., Rui, N. Z., et al. 2020a, ApJS, 247, 48, doi: 10.3847/1538-4365/ab7919

Kremer, K., Spera, M., Becker, D., et al. 2020b, arXiv e-prints, arXiv:2006.10771. https://arxiv.org/abs/2006.10771

Kroupa, P. 2001, MNRAS, 322, 231, doi: 10.1046/j.1365-8711.2001.04022.x

Kruijssen, J. M. D., Pelupessy, F. I., Lamers, H. J. G. L. M., Portegies Zwart, S. F., & Icke, V. 2011, MNRAS, 414, 1339, doi: 10.1111/j.1365-2966.2011.18467.x

Kulkarni, S. R., Hut, P., & McMillan, S. 1993, Nature, 364, 421, doi: 10.1038/364421a0

Kumar, P., Narayan, R., & Johnson, J. L. 2008, MNRAS, 388, 1729, doi: 10.1111/j.1365-2966.2008.13493.x

Kumar, P., & Zhang, B. 2015, PhR, 561, 1, doi: 10.1016/j.physrep.2014.09.008

Lada, C. J., & Lada, E. A. 2003, ARA&A, 41, 57, doi: 10.1146/annurev.astro.41.011802.094844

Law, N. M., Kulkarni, S. R., Dekany, R. G., et al. 2009, PASP, 121, 1395, doi: 10.1086/648598

Levan, A. J., Tanvir, N. R., Starling, R. L. C., et al. 2014, ApJ, 781, 13, doi: 10.1088/0004-637X/781/1/13

Liu, F. K., Li, S., & Chen, X. 2009, ApJL, 706, L133

Liu, F. K., Li, S., & Komossa, S. 2014, ApJ, 786, 103, doi: 10.1088/0004-637X/786/2/103

Lopez, Jr., M., Batta, A., Ramirez-Ruiz, E., Martinez, I., & Samsing, J. 2018, arXiv e-prints. https://arxiv.org/abs/1812.01118

Loup, C., Forveille, T., Omont, A., & Paul, J. F. 1993, A&AS, 99, 291

LSST Science Collaboration, Abell, P. A., Allison, J., et al. 2009, arXiv e-prints, arXiv:0912.0201. https://arxiv.org/abs/0912.0201

Lyutikov, M., & Toonen, S. 2019, MNRAS, 487, 5618, doi: 10.1093/mnras/stz1640

Maccarone, T. J., Kundu, A., Zepf, S. E., & Rhode, K. L. 2007, Nature, 445, 183, doi: 10.1038/nature05434

Mackey, A. D., Wilkinson, M. I., Davies, M. B., & Gilmore, G. F. 2007, MNRAS, 379, L40, doi: 10.1111/j.1745-3933.2007.00330.x

MacLeod, M., Goldstein, J., Ramirez-Ruiz, E., Guillochon, J., & Samsing, J. 2014, ApJ, 794, 9, doi: 10.1088/0004-637X/794/1/9

MacLeod, M., Guillochon, J., Ramirez-Ruiz, E., Kasen, D., & Rosswog, S. 2016, ApJ, 819, 3, doi: 10.3847/0004-637X/819/1/3

Mapelli, M. 2016, MNRAS, 459, 3432, doi: 10.1093/mnras/stw869

Margutti, R., Metzger, B. D., Chornock, R., et al. 2019, ApJ, 872, 18, doi: 10.3847/1538-4357/aafa01

Marks, M., Kroupa, P., Dabringhausen, J., & Pawlowski, M. S. 2012, MNRAS, 422, 2246, doi: 10.1111/j.1365-2966.2012.20767.x

Miller-Jones, J. C. A., Strader, J., Heinke, C. O., et al. 2015, MNRAS, 453, 3918, doi: 10.1093/mnras/stv1869

Morscher, M., Pattabiraman, B., Rodriguez, C., Rasio, F. A., & Umbreit, S. 2015, The Astrophysical Journal, 800, 9, doi: 10.1088/0004-637X/800/1/9

Pattabiraman, B., Umbreit, S., Liao, W.-k., et al. 2013, The Astrophysical Journal Supplement Series, 204, 15, doi: 10.1088/0067-0049/204/2/15

Perets, H. B., Li, Z., Lombardi, Jr., J. C., & Milcarek, Jr., S. R. 2016, ApJ, 823, 113, doi: 10.3847/0004-637X/823/2/113

Perley, D. A., Mazzali, P. A., Yan, L., et al. 2019, MNRAS, 484, 1031, doi: 10.1093/mnras/sty3420

Phinney, E. S. 1989, in The Center of the Galaxy, ed. M. Morris, Vol. 136, 543

Piro, A. L., & Lu, W. 2020, ApJ, 894, 2, doi: 10.3847/1538-4357/ab83f6
Portegies Zwart, S. F., Baumgardt, H., Hut, P., Makino, J., & McMillan, S. L. W. 2004, Nature, 428, 724, doi: 10.1038/nature02448
Portegies Zwart, S. F., McMillan, S. L. W., & Gieles, M. 2010, ARA&A, 48, 431, doi: 10.1146/annurev-astro-081309-130834
Prentice, S. J., Maguire, K., Smartt, S. J., et al. 2018, ApJL, 865, L3, doi: 10.3847/2041-8213/aadd90
Pursiainen, M., Childress, M., Smith, M., et al. 2018, MNRAS, 481, 894, doi: 10.1093/mnras/sty2309
Quataert, E., Lecoanet, D., & Coughlin, E. R. 2019, MNRAS, 485, L83, doi: 10.1093/mnrasl/slz031
Rees, M. J. 1988, Nature, 333, 523, doi: 10.1038/333523a0
Rest, A., Garnavich, P. M., Khatami, D., et al. 2018, Nature Astronomy, 2, 307, doi: 10.1038/s41550-018-0423-2
Rodriguez, C. L., Amaro-Seoane, P., Chatterjee, S., & Rasio, F. A. 2018, Physical Review Letters, 120, 151101, doi: 10.1103/PhysRevLett.120.151101
Rodriguez, C. L., Chatterjee, S., & Rasio, F. A. 2016, Physical Review D, 93, 084029, doi: 10.1103/PhysRevD.93.084029
Rodriguez, C. L., & Loeb, A. 2018, ArXiv e-prints. https://arxiv.org/abs/1809.01152
Rodriguez, C. L., Morscher, M., Wang, L., et al. 2016, MNRAS, 463, 2109, doi: 10.1093/mnras/stw2121
Rosswog, S., Ramirez-Ruiz, E., & Hix, W. R. 2009, ApJ, 695, 404, doi: 10.1088/0004-637X/695/1/404
Samsing, J. 2018, PhRvD, 97, 103014, doi: 10.1103/PhysRevD.97.103014
Samsing, J., MacLeod, M., & Ramirez-Ruiz, E. 2017, ApJ, 846, 36, doi: 10.3847/1538-4357/aa7e32
Samsing, J., Venumadhav, T., Dai, L., et al. 2019, PhRvD, 100, 043009, doi: 10.1103/PhysRevD.100.043009
Sana, H., de Mink, S. E., de Koter, A., et al. 2012, Science, 337, 444, doi: 10.1126/science.1223344
Shakura, N. I., & Sunyaev, R. A. 1973, A&A, 500, 33
Shen, R.-F., & Matzner, C. D. 2014, ApJ, 784, 87, doi: 10.1088/0004-637X/784/2/87
Shishkovsky, L., Strader, J., Chomiuk, L., et al. 2018, ApJ, 855, 55, doi: 10.3847/1538-4357/aaadb1
Sigurdsson, S. 1993, ApJL, 415, L43, doi: 10.1086/187028
Spera, M., & Mapelli, M. 2017, MNRAS, 470, 4739, doi: 10.1093/mnras/stx1576
Spitzer, L. 1987, Dynamical evolution of globular clusters
Strader, J., Chomiuk, L., Maccarone, T. J., Miller-Jones, J. C. A., & Seth, A. C. 2012, Nature, 490, 71, doi: 10.1038/nature11490
Tonry, J. L., Denneau, L., Heinze, A. N., et al. 2018, PASP, 130, 064505, doi: 10.1088/1538-3873/aabadf
van den Hoek, L. B., & Groenewegen, M. A. T. 1997, A&AS, 123, 305, doi: 10.1051/aas:1997162
Vink, J. S., de Koter, A., & Lamers, H. J. G. L. M. 2001, A&A, 369, 574, doi: 10.1051/0004-6361:20010127
Wang, L. 2020, MNRAS, 491, 2413, doi: 10.1093/mnras/stz3179
Wang, L., Spurzem, R., Aarseth, S., et al. 2015, MNRAS, 450, 4070, doi: 10.1093/mnras/stv817
Weatherford, N. C., Chatterjee, S., Kremer, K., & Rasio, F. A. 2019, arXiv e-prints, arXiv:1911.09125. https://arxiv.org/abs/1911.09125
Woosley, S. E. 2017, ApJ, 836, 244, doi: 10.3847/1538-4357/836/2/244
Ye, C. S., Kremer, K., Chatterjee, S., Rodriguez, C. L., & Rasio, F. A. 2019, arXiv e-prints. https://arxiv.org/abs/1902.05963
Yuan, F., Wu, M., & Bu, D. 2012, ApJ, 761, 129, doi: 10.1088/0004-637X/761/2/129
Ziosi, B. M., Mapelli, M., Branchesi, M., & Tormen, G. 2014, MNRAS, 441, 3703, doi: 10.1093/mnras/stu824